2017

Entropy in self-similar shock profiles

L. G. Margolin
Los Alamos National Laboratory

J. M. Reisner
Los Alamos National Laboratory

P. M. Johnson
U.S. Naval Research Laboratory, pedro.jordan@nrlssc.navy.mil

International Journal of Non-Linear Mechanics 95 (2017) 333–346

Contents lists available at ScienceDirect

International Journal of Non-Linear Mechanics

journal homepage: www.elsevier.com/locate/nlm

Entropy in self-similar shock profiles

L.G. Margolin [a], J.M. Reisner [a], P.M. Jordan [b,*]

[a] Computational Physics Division, Los Alamos National Laboratory, MS F644, Los Alamos, NM 87545, USA
[b] Acoustics Division, U.S. Naval Research Laboratory, Stennis Space Center, MS 39529, USA

ARTICLE INFO

Keywords:
Becker's solution
Entropy
Shock structure
Navier–Stokes equations

ABSTRACT

In this paper, we study the structure of a gaseous shock, and in particular the distribution of entropy within, in both a thermodynamics and a statistical mechanics context. The problem of shock structure has a long and distinguished history that we review. We employ the Navier–Stokes equations to construct a self-similar version of Becker's solution for a shock assuming a particular (physically plausible) Prandtl number; and that solution reproduces the well-known result of Morduchow & Libby that features a maximum of the equilibrium entropy inside the shock profile. We then construct an entropy profile, based on gas kinetic theory, that is smooth and monotonically increasing. The extension of equilibrium thermodynamics to irreversible processes is based in part on the assumption of local thermodynamic equilibrium. We show that this assumption is not valid except for the weakest shocks. We conclude by hypothesizing a thermodynamic nonequilibrium entropy and demonstrating that it closely estimates the gas kinetic nonequilibrium entropy within a shock.

Published by Elsevier Ltd.

1. Introduction

1.1. Aim and scope

In this paper we will consider the entropy profile in a gaseous shock from two points of view, first that of nonequilibrium thermodynamics and second from that of gas kinetic theory. We will begin by reviewing and generalizing the classic paper of Morduchow & Libby [1] in which steady-state shock solutions of the Navier–Stokes equations are analyzed for a particular Prandtl number. Our results confirm and extend those of [1], namely, that the thermodynamic (equilibrium) entropy has a maximum inside the shock for all finite values of Prandtl number and all Mach numbers. Next, we will reconsider the problem from the point of view of nonequilibrium statistical mechanics and kinetic theory. We will calculate the Boltzmann entropy in the shock using the Grad velocity distribution function that underlies the derivation of the Navier–Stokes equations and show that it is a smooth monotonically increasing function in the shock profile.

Boltzmann's entropy is a true nonequilibrium entropy, evaluated for nonequilibrium solutions of the Boltzmann equation. However, the thermodynamic entropy is derived specifically from equilibrium statistics; it is extended to nonequilibrium systems through the assumption of local thermodynamic equilibrium (LTE). Based on experimental measurements, a gaseous shock is only a few mean free paths wide, implying that there are not sufficient collisions occurring within the shock to restore equilibrium. Using our Navier–Stokes solutions, we evaluate the LTE assumption and show that it is justified only for the weakest shocks. We conclude the paper with a proposal for a nonequilibrium thermodynamic entropy more relevant to shock analyses.

Solving for the shock profile in monatomic gases (e.g., Ar, He, Ne, Rn) is perhaps the most straightforward problem to test model predictions because the bulk viscosity coefficient in this class of gases is zero. Further, there exists good experimental data against which model results/predictions can be evaluated. There is broad agreement now that the validity of Navier–Stokes theory is restricted to rather weak shocks, i.e., those with a Mach numbers less than 2; see, e.g., [2,3]. Nevertheless, in this paper we will continue to explore Navier–Stokes theory to contribute to an understanding of the details of its breakdown.

In the next subsection, we present a brief history of the application of Navier–Stokes theory to the determination of shock profiles, our focus being on two classic works in the field: the 1922 paper of Becker [4] and the 1949 paper of Morduchow & Libby [1].

1.2. A brief history of shock profile theory

The determination of a shock's profile, i.e., the spatial dependence of density, velocity and internal energy, and its characterization by the metric known as the shock width, is a well-studied problem with an

* Corresponding author.
E-mail address: pedro.jordan@nrlssc.navy.mil (P.M. Jordan).

http://dx.doi.org/10.1016/j.ijnonlinmec.2017.07.003
Received 8 December 2016; Received in revised form 3 July 2017; Accepted 5 July 2017
Available online 16 July 2017
0020-7462/Published by Elsevier Ltd.

extensive, multi-disciplinary literature; a recent survey can be found in [5]. That literature started with the articles of Rayleigh [6] and Taylor [7], both in 1910, in which the general one-dimensional (1D) equation of motion for the Navier–Stokes shock profile was first derived; these authors, however, were only able to obtain solutions for either the constant viscosity-only or the constant heat conductivity-only special case. It was Becker [4] who, in 1922, was the first to publish a steady-shock solution of the (compressible) Navier–Stokes equations wherein both viscosity and heat conduction were taken into account. The main point of Becker's article was to raise important questions concerning the validity of the Navier–Stokes equations in the study of strong shocks.

The Becker solution is a special case result; the stationary shock profile he derived assumes a particular Prandtl number, namely, $Pr = 3/4$, which is a reasonable value for many gases. (For quantitative discussions of this approximation, see [8] for large Mach numbers and [9] for small Mach numbers). The solution presumes an infinite 1D gaseous medium with inflow at one end and outflow at the other. The shock is stationary in the chosen reference frame, and so the problem is one of steady flow. The solution, however, is not *a priori* Galilean invariant; when the shock is stationary, no net work is done on the system, while in every other reference frame this is not so. Also, as the number of required conditions behind the shock is different, it is not clear whether the steady-shock solution is equivalent to the one obtained via the traveling wave assumption—specifically, while both approaches assume the vanishing of the velocity gradient at the inflow end, the steady solution (in, say, [1]) requires that both the velocity (i.e., piston velocity) *and* temperature be specified there, whereas the only inflow datum to be specified for the traveling wave solution is the piston velocity. However, our analysis indicate the *qualitative* equivalence of the two methodologies to within a Galilean transformation.

Becker's 1922 paper [4] was the first in which a shock profile solution that included the effects of *both* viscosity and heat conduction was derived; here, however, we have modeled our investigation on that of Morduchow & Libby [1], who revisited and refined Becker's analysis in 1949. We have chosen to work consistently with (specific) internal energy $\mathcal{E}$, rather than temperature, and to deal with equations written in conservative form. To facilitate comparison with our computer simulation results, rather than with experiment, we will maintain the dependence on the (longitudinal) fluid viscosity $\bar{\mu}$ and the thermal coefficient κ rather than introduce kinetic theory estimates of these parameters as was done in [1]. These parameters appear in the Navier–Stokes equations (1)–(3) and their relation to Morduchow& Libby's parameters μ and k is described in footnote 1. In our analyses, it is more convenient to work with the (dimensionless) parameter $\mathcal{P} = \kappa/\bar{\mu}$, which can also be written as $\mathcal{P} = \gamma/Pr''$. Here, Pr'' represents the *longitudinal Prandtl number* (see Hayes [10, p. 39]) and $\gamma \in (1, 5/3]$ denotes the ratio of specific heats.

As noted by Morduchow& Libby in their 1965 paper [11], "the fact that entropy does not increase monotonically through the shock has apparently been discovered independently at least four different times from 1944–1961". Precedence in this regard must be, however, given to Roy [12], who solved the Navier–Stokes equations using a generalization of Becker's assumption that extended to certain non-monatomic gases, but who curiously did not cite Becker's work. Morduchow & Libby [1], on the other hand, generalize Becker's work by including temperature dependence in the viscous and thermal conduction coefficients. The later papers of Golitsyn & Staniukovich [13] and of Serrin & Whang [14] on this topic employ more general thermodynamic arguments that do not depend on Becker's assumption. Based on citations, only [1] appears to be well known in the shock-physics community.

1.3. Outline of paper

This paper is primarily concerned with the distribution of entropy in a gaseous shock and is conceptually broken into two parts. In Sections 2 through 5 we will work in the context of thermodynamics and the compressible Navier–Stokes equations. In Sections 6 through 8 we will transition to the more fundamental descriptions of statistical mechanics and gas kinetic theory.

In Section 2, we derive the equations for a self-similar shock wave including both viscosity and heat conduction. For the specific case of $\mathcal{P} = \gamma$, we obtain an integrable ODE that yields exact solutions for the velocity, density, energy, and entropy profiles corresponding to (what we term) the "full physics" Navier–Stokes equations, by which we mean the system of nonlinear flow equations that includes both (physical) viscosity and heat conduction. In Section 3, we prove that, as functions of our similarity variable, the first three listed field variables have monotone profiles. We also reproduce the result in [1] showing that the equilibrium entropy, defined in Eq. (26) below, exhibits a maximum inside the shock region, and we determine its location. In Section 4, we derive a class of explicit traveling wave solutions for special case values of the Mach number.

Section 5 is concerned with numerical simulations. We describe a high-resolution code that integrates the Navier–Stokes equations for a piston-driven shock. The resolution is high enough that physical viscosity and heat conduction alone are sufficient to ensure stable solutions; i.e., no artificial viscosity [15,16] is required. We compare the analytical (self-similar) and numerical profiles, verifying the code and verifying the stability of the (numerical) Navier–Stokes solutions.

Section 6 is concerned with the Clausius–Duhem inequality and the classical extensions of irreversible thermodynamics. Here, we introduce the fundamental nature of the local thermodynamic equilibrium (LTE) hypothesis. In Section 7, we combine the macroscopic Navier–Stokes solutions with kinetic theory to show that LTE is not a valid assumption for any but the weakest shocks. Then, in Section 8, we employ a purely statistical mechanical definition to calculate the nonequilibrium entropy profile in a shock. We conclude the paper with a summary of our findings in Section 9.

Most of the results presented in the first part of this paper are formulated in the context of Becker's assumption of a particular Prandtl number. In an effort to show that those results are more generally valid, we have added three appendices. Appendix A describes some approximate and asymptotic results for the equation of motion in Eq. (17). Appendix B gives an equation of motion and related expressions that are valid for arbitrary Prandtl number values. And in Appendix C, we develop a perturbation solution for the region near the piston's face. The findings derived from this approximation are consistent with those of Serrin & Whang [14] regarding the existence of an entropy peak for all realizable values of the Prandtl number.

2. The self-similar version of Becker's solution

It is convenient for the purposes of this paper to use a traveling wave (i.e., self-similar) *ansatz* that is more easily compared with numerical simulations of the piston-driven shock. As noted above, the steady-shock and self-similar solutions turn out to be related by a Galilean transformation; however, a derivation of the full physics version of the latter has, apparently, not been carried out previously.

Now, the (full physics) Navier–Stokes equations in one spatial dimension read

$$\frac{\partial \rho}{\partial t} + \frac{\partial}{\partial x}[\rho u] = 0, \tag{1}$$

$$\frac{\partial \rho u}{\partial t} + \frac{\partial}{\partial x}\left[\rho u^2 + p - \bar{\mu}\frac{\partial u}{\partial x}\right] = 0, \tag{2}$$

$$\frac{\partial}{\partial t}\left[\rho\mathcal{E} + \frac{1}{2}\rho u^2\right] + \frac{\partial}{\partial x}\left[\rho u\mathcal{E} + \frac{1}{2}\rho u^3 + pu - \bar{\mu}\,u\frac{\partial u}{\partial x} - \kappa\frac{\partial \mathcal{E}}{\partial x}\right] = 0. \tag{3}$$

And to close this system, we assume the well known equation of state [17, §2.5]

$$p = (\gamma - 1)\rho\mathcal{E}. \tag{4}$$

Here, ρ, u, p and $\mathcal{E}$ have their usual meanings of mass density, velocity, pressure, and specific internal energy; we have used the fact that $\mathcal{E} = c_v T$

in perfect gases, where $T > 0$ is the absolute temperature and c_v is the (assumed constant) specific heat at constant volume; we have also assumed that $\mathbf{q}$, the heat flux vector, obeys Fourier's law [17, p. 29]. As is well known, $\bar{\mu}$ and κ, the transport coefficients,[1] depend on T; in actuality, this dependence is quantitatively significant in increasing the shock width (see, e.g., [18]), but including that dependence complicates the analysis while introducing little qualitative effect. Hence, unless otherwise indicated, we shall assume $\bar{\mu}$ and κ to be constants.

The traveling wave equations result from assuming that all field variables depend on only the similarity variable $y = x - vt$, where the constant v will turn out to be the shock velocity. Applying the similarity assumption to Eqs. (1)–(4) leads to

$$\frac{d}{dy}\left[-v\rho + u\rho\right] = 0, \tag{5}$$

$$\frac{d}{dy}\left[-vu\rho + u^2\rho + p - \bar{\mu}\frac{du}{dy}\right] = 0, \tag{6}$$

$$\frac{d}{dy}\left[-v\rho\mathcal{E} + u\rho\mathcal{E} - \frac{1}{2}\rho u^2 v + \frac{1}{2}\rho u^3 + pu - u\bar{\mu}\frac{du}{dy} - \kappa\frac{d\mathcal{E}}{dy}\right] = 0, \tag{7}$$

$$p = (\gamma - 1)\rho\mathcal{E}. \tag{8}$$

Integrating (5)–(7) and then solving for the resulting constants of integration by imposing and enforcing the right–asymptotic conditions

$$\rho \to \rho_o, \qquad u \to 0, \qquad \mathcal{E} \to \mathcal{E}_o, \qquad p \to p_o,$$

$$\frac{du}{dy} \to 0, \qquad \frac{d\mathcal{E}}{dy} \to 0 \qquad (y \to \infty),$$

which correspond to a shock moving to the *right*, yields

$$\rho(v - u) = \rho_o v, \tag{9}$$

$$u\rho(v - u) - (\gamma - 1)\rho\mathcal{E} + \bar{\mu}\frac{du}{dy} = -p_o, \tag{10}$$

$$\rho\mathcal{E}(v - u) + \frac{1}{2}\rho u^2(v - u) - (\gamma - 1)\rho\mathcal{E}u + \bar{\mu}u\frac{du}{dy} + \kappa\frac{d\mathcal{E}}{dy} = v\mathcal{E}_o\rho_o. \tag{11}$$

where we observe that $p_o = (\gamma - 1)\rho_o\mathcal{E}_o$.

We now multiply the momentum equation (10) by v and then subtract it from the energy equation (11). This yields, after simplifying with Eq. (9),

$$\gamma\rho_o v\mathcal{E} + \rho_o v\left(\frac{1}{2}u^2 - uv\right) - (v - u)\bar{\mu}\frac{du}{dy} + \kappa\frac{d\mathcal{E}}{dy} = \gamma\rho_o v\mathcal{E}_o, \tag{12}$$

which, after some additional manipulation, becomes

$$\gamma\mathcal{E} + \frac{1}{2}(v - u)^2 + \left(\frac{1}{\rho_o v}\right)\frac{d}{dy}\left[\kappa\mathcal{E} + \frac{\bar{\mu}}{2}(v - u)^2\right] = \gamma\mathcal{E}_o + \frac{1}{2}v^2. \tag{13}$$

Clearly, Eqs. (9), (10) and (13) apply for all Mach and Prandtl numbers. At this point, however, we make the assumption of a particular $\mathcal{P}$, namely, $\mathcal{P} = \gamma$ (i.e., $\kappa = \gamma\bar{\mu}$). Consequently, Eq. (13) becomes

$$\left[\gamma\mathcal{E} + \frac{1}{2}(v - u)^2\right] + \left(\frac{\bar{\mu}}{\rho_o v}\right)\frac{d}{dy}\left[\gamma\mathcal{E} + \frac{1}{2}(v - u)^2\right] = \gamma\mathcal{E}_o + \frac{1}{2}v^2, \tag{14}$$

which immediately integrates to

$$\left(\gamma\mathcal{E} + \frac{1}{2}(v - u)^2\right) = \widetilde{B} + C_4\exp\left(-\rho_o v\int\frac{dy}{\bar{\mu}}\right), \tag{15}$$

where we have set $\widetilde{B} \equiv \gamma\mathcal{E}_o + v^2/2$. Note that C_4, the constant of integration, must vanish to prevent the blow-up of the exponential in Eq. (15) as $y \to -\infty$. Upon setting $C_4 = 0$, the RHS of Eq. (15) reduces to a *constant*, and thus we recover the classic result

$$\gamma\mathcal{E} + \frac{1}{2}(v - u)^2 = \widetilde{B}, \tag{16}$$

i.e., the total enthalpy becomes a constant for $\mathcal{P} = \gamma$; see, e.g., [10].

[1] In [1], μ is the shear viscosity and k is the heat conductivity, where in the case of monatomic gases $\mu = 3\bar{\mu}/4$; see [10], wherein $\bar{\mu}$ is termed the *longitudinal coefficient of viscosity*. Here, we have set $\kappa = k/c_v$. Thus, $\mathcal{P} = \gamma$ is equivalent to taking $Pr = 3/4$ in [4] and [1].

Next, we solve Eq. (16) for $\mathcal{E}$ and substitute into the momentum equation (10). After then eliminating the density from the latter using Eq. (9), followed by some additional manipulation, we end up with the following Abel ODE as our equation of motion:

$$\ell w\frac{dw}{dy} = -(w - 1)(w - \alpha) \qquad (\mathcal{P} = \gamma). \tag{17}$$

In Eq. (17), we have defined $w \equiv 1 - u/v$; the length scale

$$\ell \equiv \left(\frac{\bar{\mu}}{\rho_o v}\right)\left(\frac{2\gamma}{\gamma + 1}\right); \tag{18}$$

and the dimensionless constant

$$\alpha \equiv \frac{\gamma - 1}{\gamma + 1} + \frac{2}{(\gamma + 1)\mathcal{M}^2}, \tag{19}$$

where we have introduced the Mach number, $\mathcal{M} \equiv v/c_o$, and the sound speed ahead of the shock, $c_o = \sqrt{\gamma(\gamma - 1)\mathcal{E}_o}$.

The shock velocity v is determined from Eq. (17) by applying and enforcing the left-asymptotic conditions on u, specifically,

$$u \to u_p, \qquad \frac{du}{dy} \to 0 \qquad (y \to -\infty),$$

which in terms of w become

$$w \to 1 - u_p/v, \qquad \frac{dw}{dy} \to 0 \qquad (y \to -\infty),$$

where $u_p > 0$ is the (constant) speed of the piston. This leads to the quadratic equation

$$v^2 - \frac{\gamma + 1}{2}u_p v - c_o^2 = 0. \tag{20}$$

Thus, for a shock moving to the right

$$v = \frac{\gamma + 1}{4}u_p + \sqrt{\left(\frac{\gamma + 1}{4}u_p\right)^2 + c_o^2} > u_p, \tag{21}$$

where the inequality follows from the thermodynamic constraint $\gamma > 1$, and from which it is easy to see that $\mathcal{M} > 1$.

It should be noted that on eliminating c_o^2 between Eqs. (19) and (20), the latter reduces to

$$\alpha = 1 - \frac{u_p}{v}, \tag{22}$$

which we recall is the left–asymptotic limit of w. In addition, it is readily established that $0 < \alpha < 1$.

Note that for arbitrary (realizable) values of α, Eq. (17) can be integrated to yield an exact solution for w. While this solution is, in general, in implicit form, for at least one special case value of α, an explicit expression can be obtained; see Section 4 below, where we exhibit and discuss this special class of solutions.

Now, it is useful to write the other field variables in terms of the velocity. From Eq. (9), we have the general result

$$\rho = \frac{\rho_o}{w}. \tag{23}$$

For the particular choice of $\mathcal{P} = \gamma$, we derive from Eq. (16)

$$\mathcal{E} = \mathcal{E}_o\left[1 + \frac{\gamma - 1}{2}\mathcal{M}^2\left(1 - w^2\right)\right]. \tag{24}$$

Using Eq. (8), the equation of state, in Eq. (24) then gives us

$$p = \frac{p_o}{w}\left[1 + \frac{\gamma - 1}{2}\mathcal{M}^2\left(1 - w^2\right)\right]. \tag{25}$$

Recasting [17, eq. (2.83)] in terms of ρ and $\mathcal{E}$, we take the change in the *equilibrium* (specific) entropy S of an perfect gas to be given by

$$\frac{S - S_o}{c_v} = \ln\left(\frac{\mathcal{E}}{\mathcal{E}_o}\right) - (\gamma - 1)\ln\left(\frac{\rho}{\rho_o}\right), \tag{26}$$

which after making use of Eqs. (23)–(25) becomes

$$\frac{S - S_o}{c_v} = \ln\left[1 + \frac{\gamma - 1}{2}\mathcal{M}^2(1 - w^2)\right] + (\gamma - 1)\ln[w]. \tag{27}$$

3. Profiles

It is not necessary to have explicit solutions to Eq. (17) to determine whether each of the profiles (i.e., those of u, ρ, $\mathcal{E}$, and S) is a monotone function of y; indeed, establishing such is not difficult. First, we show that the velocity must be a monotone function of y using proof by contradiction.[2]

- From Eq. (21), $v > u_p \geq u$; so the monotonicity of w implies the monotonicity of u.
- Assume now that w has a maximum, w_m, at some finite value $y = y_m$; then at that point $\frac{dw}{dy}|_{y=y_m} = 0$.
- Then from Eq. (17), either $w_m = 1$ or $w_m = \alpha$. Assume $w_m = 1$.
- If w_m is an absolute maximum, then the slope must change sign from one side to the other. Thus, on one side of the maximum, the slope must be positive.
- From Eq. (17), a positive slope implies then that $w > 1$.
- This, however, contradicts the assumption that $w_m = 1$ is the maximum value.
- A similar argument shows that there cannot be a minimum in the profile.
- Thus, the w vs. y profile is a kink, i.e., a monotone function of y. The slope $\frac{dw}{dy} > 0$ everywhere, but tends to zero at the asymptotic limits $y \to \pm\infty$.

Consider next the density profile. From Eq. (23)

$$\frac{d\rho}{dy} = \frac{d\rho}{dw}\frac{dw}{dy} = -\frac{\rho_o}{w^2}\frac{dw}{dy} \leq 0.$$

That is, density is monotonically increasing with increasing w or equivalently with decreasing y. Similarly, from Eq. (24)

$$\frac{d\mathcal{E}}{dy} = \frac{d\mathcal{E}}{dw}\frac{dw}{dy} = -\frac{(\gamma-1)\mathcal{M}^2}{2}\left(2w\mathcal{E}_o\right)\frac{dw}{dy} \leq 0,$$

so $\mathcal{E}$ is also monotonically increasing with increasing w or, equivalently, with decreasing y.

As reported in [1,12], the equilibrium entropy of Becker's solution does exhibit a maximum. From Eq. (27)

$$\frac{dS}{dy} = \frac{dS}{dw}\frac{dw}{dy} = (\gamma-1)\,c_v\left[\frac{-w\mathcal{M}^2}{1+\frac{\gamma-1}{2}\mathcal{M}^2(1-w^2)} + \frac{1}{w}\right]\frac{dw}{dy},$$

which has an interior zero at

$$w_m = \frac{1}{\mathcal{M}}\sqrt{\frac{2+(\gamma-1)\mathcal{M}^2}{(\gamma+1)}} = \sqrt{\alpha}. \tag{28}$$

Here, we note that $w_m \to 1$ as $\mathcal{M} \to 1$. For stronger shocks, w_m decreases monotonically and asymptotes to $\sqrt{\frac{\gamma-1}{\gamma+1}}$ as $\mathcal{M} \to \infty$. To summarize, in every shock solution (for the special case $\mathcal{P} = \gamma$) with $1 < \mathcal{M} < \infty$, Eq. (27) has an interior maximum, and $w_m \in (\frac{1}{2}, 1)$ in perfect gases.

Plots of the velocity and the entropy versus the similarity coordinate are shown in Figs. 1 and 2 for the self-similar Becker solution with $\mathcal{M} = \sqrt{3}$ and $\gamma = 5/3$ (see Section 4 below). Clearly, the velocity profile is a kink, monotonically decreasing to the right; in contrast, the entropy profile exhibits a maximum, which in this case occurs at $w_m = 1/\sqrt{2}$.

4. A special solution

On separating variables and performing a partial-fraction decomposition, the Becker equation of motion (i.e., Eq. (17)) becomes

$$\left(\frac{\alpha}{w-\alpha} - \frac{1}{w-1}\right)dw = -\left(\frac{\alpha-1}{\ell}\right)dy. \tag{29}$$

The position of the shock is not specified in our statement of the problem; here, we will place the center of the shock, defined as the point where $u = \frac{1}{2}u_p$, at $y = 0$. The integration of Eq. (29) subject to this condition then yields the (exact) solution

$$\ln\left(\frac{w-\alpha}{w_o-\alpha}\right)^{\alpha} - \ln\left(\frac{1-w}{1-w_o}\right) = -\left(\frac{\alpha-1}{\ell}\right)y \tag{30}$$

where we have set

$$w_o = w(0) \equiv 1 - \frac{u_p}{2v}. \tag{31}$$

The velocity solution derived above is, of course, implicit. In general, it is not possible to find an exact expression giving w as a function of y; see, however, Appendix A, wherein explicit approximate/asymptotic expressions are given. In this section we show that the special case $\alpha = 1/2$ yields a class of explicit, exact solutions, valid for all realizable γ. First, let us interpret this special case in terms of shock strength (i.e., Mach number). From Eq. (22) it is easily established that $\alpha = 1/2$ implies that $\mathcal{M} = \mathcal{M}^*$, where

$$\mathcal{M}^* \equiv \frac{2}{\sqrt{3-\gamma}} \qquad (1 < \gamma \leq 5/3), \tag{32}$$

from which it is clear that $\sqrt{2} < \mathcal{M}^* \leq \sqrt{3}$ in perfect gases.

In the case of monatomic gases we have

$$\mathcal{M}^* = \sqrt{3} \qquad (\gamma = 5/3),$$

and from Eqs. (22) and (31) we find that

$$w_o = 3/4 \qquad (\alpha = 1/2).$$

Substituting these particular values into Eq. (30) yields:

$$\frac{(w-1/2)^{1/2}}{(1-w)} = 2\exp\left(\frac{y}{2\ell}\right) \equiv \mathcal{X}(y). \tag{33}$$

Squaring the above equation leads to a quadratic equation for w, specifically,

$$\mathcal{X}^2w^2 - w(1+2\mathcal{X}^2) + (\mathcal{X}^2 + \frac{1}{2}) = 0, \tag{34}$$

the physically admissible solution of which (as we shall see) is

$$w = 1 + \frac{1}{2\mathcal{X}^2}\left[1 - \sqrt{1+2\mathcal{X}^2}\right], \tag{35}$$

or

$$u = \frac{v}{8}\exp\left(-\frac{y}{\ell}\right)\left[\sqrt{1+8\exp\left(\frac{y}{\ell}\right)} - 1\right]. \tag{36}$$

It is simple matter to check that this solution satisfies the imposed asymptotic conditions:

- when $y \to \infty$, $\mathcal{X} \to \infty$, so $w \to 1$ and $u \to 0$, ✓
- when $y \to -\infty$, $\mathcal{X} \to 0$, so $w \to 1/2$ and $u \to v/4 = u_p$, ✓

while at the origin,

- when $y = 0$, $\mathcal{X} = 2$, so $w_o = 3/4$ and $u = u_p/2$. ✓

The analytically determined velocity and entropy profiles derived from Eq. (36) are shown in Figs. 1 and 2.

Remark 1. For $\mathcal{P} = 0$ (i.e., $k = 0$), Eq. (B.1) reduces to

$$\ell w\frac{dw}{dy} = -\gamma(w-1)(w-\alpha) \qquad (\mathcal{P} = 0). \tag{37}$$

Thus, like Eqs. (17), (37) yields a class of exact, explicit, solutions for $\alpha = 1/2$, all members of which being easily obtained from Eq. (36) by replacing ℓ with ℓ/γ. Comparing the $\mathcal{P} = \gamma$, 0 special cases highlights the fact that neglecting heat conduction (i.e., setting $k = 0$) reduces the shock width; see Section 5.4 below.

[2] A more general theorem proving monotonicity is given in [19].

5. Numerical simulations

In this section, we present numerical solutions of a piston-driven shock. Our goals are threefold. First, we demonstrate the stability of the numerically calculated shock profile and compare it with the (analytically-derived) self-similar version of Becker's solution. (The stability of the shock is an essential input to the discussion in Section 7.) Second, we demonstrate the ability of Eulerian-framework codes to accurately reproduce analytically determined shock profiles in the direct numerical simulation (DNS) regime. And third, we offer additional verification of the code, apart from the analytical solutions, as limited justification for using this numerical program in regimes where exact expressions for the former are unknown, or otherwise unobtainable. We begin by summarizing the algorithmic program and problem setup.

5.1. A simple Eulerian program

Our simulations use the HIGRAD [20] program, which solves the multi-dimensional Euler (fluid) equations on an Eulerian mesh. We have modified the program to solve Navier–Stokes equations by adding both physical viscosity and heat conduction. There are many highly effective algorithms for treating shocks in the under-resolved regime where one solves the Euler equations regularized by either implicit or explicit artificial viscosity. In the highly resolved calculations described below, physical viscosity and heat conduction provide sufficient dissipation so that no regularization is required. In particular, our algorithm uses centered spatial differences in flux (conservation) form. The explicit time marching scheme is centered over the time-step by a third-order Runge–Kutta approximation. Further details of the HIGRAD program are described in [20].

Each calculation uses a fixed cell size and a fixed time step. The discrete equations approximate the 1D Navier–Stokes equations (1)–(4). We use internal energy rather than temperature, but note that for a perfect gas, the former is proportional to the latter with the constant of proportionally being c_v.

5.2. Problem set-up

Our problems simulate a steady piston-driven shock in a stationary perfect gas. The flow is self-similar and is characterized by a single flow parameter, the Mach number, and by the initial conditions. The fluid properties are characterized by the parameters γ, $\bar{\mu}$, and κ.

We define a problem domain of length 20.0 μm with an individual cell size $\eth x = 100$ nm. We initialize the problem by specifying two material states separated by a membrane. Most of the problem domain lies to the right of the membrane and consists of a stationary gas with density, velocity and internal energy $(\rho_R, u_R, \mathcal{E}_R)$. Correspondingly, to the left of the membrane we set $(\rho_L, u_L, \mathcal{E}_L)$. We define $c_R \equiv \sqrt{\gamma(\gamma-1)\mathcal{E}_R}$ and write the Mach number as $\mathcal{M} = v/c_R$, where we recall that v is the shock speed. Note that c_R is the same as c_o, the sound speed ahead of the shock; see Section 2.

To initialize the shock, we relate these quantities by the Rankine–Hugoniot equations. When the gas on the right is stationary ($u_R = 0$), these relations are simply written in terms of the Mach number:

$$\frac{u_L}{c_R} = \frac{2(\mathcal{M}^2-1)}{(\gamma+1)\mathcal{M}}, \qquad \frac{\rho_L}{\rho_R} = \frac{\gamma+1}{\gamma-1+2\mathcal{M}^{-2}},$$
$$\frac{\mathcal{E}_L}{\mathcal{E}_R} = \left[1+\frac{2\gamma}{\gamma+1}(\mathcal{M}^2-1)\right]\left[\frac{\gamma-1+2\mathcal{M}^{-2}}{\gamma+1}\right]. \tag{38}$$

In addition, to support the shock forward in time, new material in the same 'L–state' is fluxed into the mesh on the left boundary with shock speed v.

More specifically, we assume the gas to be argon, a monatomic gas, meaning that $\gamma = 5/3$, and we use a (constant) viscosity value of $\bar{\mu} = 2.94 \cdot 10^{-5}$ kg/(m s) and take $\mathcal{P} = 5/3$. Also, we assume $\rho_R = 1.0$ kg/m^3, $u_R = 0$, and $\mathcal{E}_R = 9.048{\cdot}10^4$ m^2/s^2 in the gas to the right of the membrane.

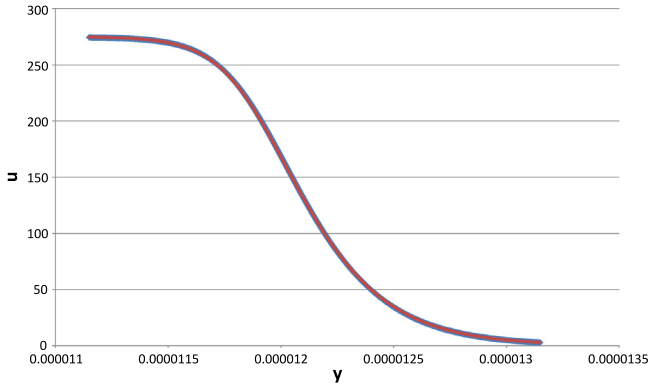

Fig. 1. Red curve: u vs. similarity coordinate (y) plotted from the special solution of Section 4. Blue curve: numerical simulation of the velocity field generated using HIGRAD (see Section 5) to solve the 1-D Navier–Stokes system for the same parameter values assumed in Section 4. (For interpretation of the references to color in this figure legend, the reader is referred to the web version of this article.)

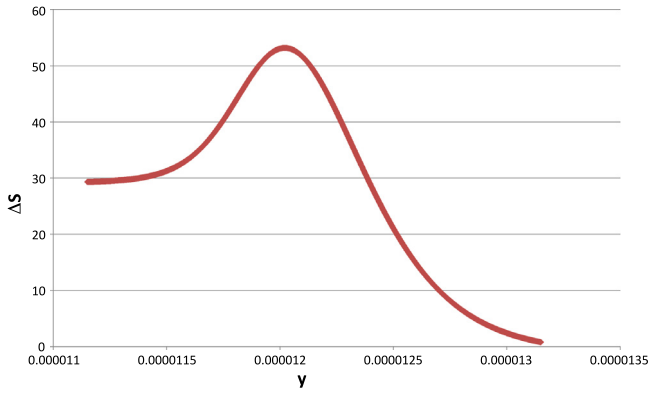

Fig. 2. Red curve: ΔS vs. y profile, where $\Delta S \equiv (S - S_o)/c_v$, corresponding to the special solution of Section 4. Blue curve: numerical simulation of the ΔS profile generated from the HIGRAD velocity field data plotted in Fig. 1. (For interpretation of the references to color in this figure legend, the reader is referred to the web version of this article.)

Note that T does not appear in our calculations; however, we use the specific heat value $c_v = 312$ m^2/(s^2 K), which corresponds a temperature of approximately 290 K, as the ambient temperature to the right of the membrane. To simulate the special solution of Section 4, we set $\mathcal{M} = \sqrt{3}$ in Eq. (38) to derive the state conditions of the shocked gas $(\rho_L, u_L, \mathcal{E}_L)$.

We devote 300 cells to the shocked material left of the membrane and run the problem for several thousand cycles to establish a numerically steady shock profile. We use a constant time-step of $4.0{\cdot}10^{-15}$ s. And even though the simulations are one-dimensional, we typically employed 500 processors to complete a given run in a reasonable amount of "wall clock" time.

5.3. Numerical results

We begin with comparisons of the code predictions with those of the (explicit) solution derived in Section 4. Using the parameter values noted above and Eq. (18), we find the length scale in Eq. (36) to be $\ell \approx 66.9$ nm. In Fig. 1 we compare the two velocity profiles. Note that there are *two* graphs in this figure, indistinguishable in the view-graph norm. As noted at the end of Section 2, ρ, $\mathcal{E}$, and S, can all be written as functions of the velocity, so it is clear that the close agreement of the velocity profiles seen here implies similar agreement vis-à-vis those of the other field variables. However, for completeness, and later reference, we show the comparison of the entropy profiles in Fig. 2.

5.4. Kinetic estimates

Using [1, eq. (9b)], we estimate the mean free path in the pre-shocked gas for the conditions listed above as

$$\lambda_R = \frac{3}{4}\sqrt{\frac{\gamma\pi}{8}}\left(\frac{\bar{\mu}}{\rho_R c_R \delta}\right)\Bigg|_{\delta=0.35} \approx 160.7 \text{ nm}, \tag{39}$$

where $1/3 \le \delta \lesssim 0.499$ [1, p. 676]. A similar estimate of 114.6 nm is obtained using the formula in a footnote of Alsmeyer [2, p. 499], which we observe follows on setting $\delta = 5\pi/32$ (≈ 0.491) in Eq. (39); see also [17, §2.7].

A typical estimate of the shock width, which we denote here by $\mathcal{W}(> 0)$, is given by

$$\mathcal{W} \equiv \frac{u_L - u_R}{|s|}. \tag{40}$$

Here, $|s|$ is the magnitude of the velocity profile's slope at the *midpoint* of the shock, i.e.,

$$s \equiv \left.\frac{du}{dy}\right|_{u=u^*}, \quad \text{where } u^* \equiv \frac{1}{2}(u_L + u_R).$$

(In the case of Eq. (17), $u^* = v(1-\alpha)/2$.) For the case of the special solution in the previous section, where $\mathcal{M} = \sqrt{3}$, one has $\alpha = 1/2$, $u_L = v(1-\alpha) = v/2$, $u_R = 0$, and $u^* = v/4$. Now from Eq. (17) one calculates $|s| = v/(12\ell)$, so that $\mathcal{W} = 6\ell$; but, as noted above, $\ell \approx 66.9$ nm. Consequently, the theoretical value of the shock width for the special solution is

$$\boxed{\mathcal{W} \approx 401.5\text{nm}.} \tag{41}$$

(For the version of the special solution corresponding to Eq. (37), $\mathcal{W} = 6\ell/\gamma \approx 240.9$ nm.) Thus, Eq. (39) implies that the width of the $\mathcal{M} = \sqrt{3}$ shock in argon is approximately 2.5 and 3.5 mean free paths for $\delta = 0.35, 5\pi/32$, respectively, in the case of Becker's solution.

5.5. Shock widths for three conduction cases

Experimental results reported in [2,3], both of which take $\delta = 5\pi/32$, indicate that in argon the thinnest shocks have a width of about 3 mean free paths and first occur for $\mathcal{M} \approx 3$. In Fig. 3 (velocity) and 4 (energy), we illustrate the additional widening of the Mach 3 shock due to the inclusion of heat conduction and the temperature-dependence of $\bar{\mu}, \kappa$. We consider three models: (I) there is viscosity but no heat conduction, i.e., $\mathcal{P} = 0$ (see Eq. (37)); (II) there is constant viscosity and heat conductivity such that $\mathcal{P} = \gamma$ (i.e., the Becker case); and (III), both the viscosity and heat conductivity coefficients are power-law functions of temperature, specifically, $\bar{\mu}, \kappa \propto T^{0.68}$, where we have employed the exponent used by Schmidt [3]. The shock width can be estimated in terms of the gradients of velocity, density or specific internal energy, and these lead to similar, but quantitatively different, results.

In the more physically realistic case of temperature-dependent viscosity and conductivity (i.e., case (III)), we see the $\mathcal{M} = 3$ velocity profile admits a shock width of approximately 3 and 4 mean free paths for $\delta = 0.35, 5\pi/32$, respectively. We also note that the energy profile is strongly skewed; i.e., the leading part of the shock is flattened much more significantly than the back of the shock. Schmidt also notes that Navier–Stokes theory produces shocks that are more asymmetric than what is seen in experiments; see Appendix A.1 where the asymmetric form of the self-similar version of Becker's solution is established for all realizable $\mathcal{M}$.

5.6. Comparisons of perturbation solutions at the back of the shock

In Appendix C we derive a perturbation solution for $\mathcal{E}$ as a function of velocity near the back of the shock, i.e., corresponding to the piston

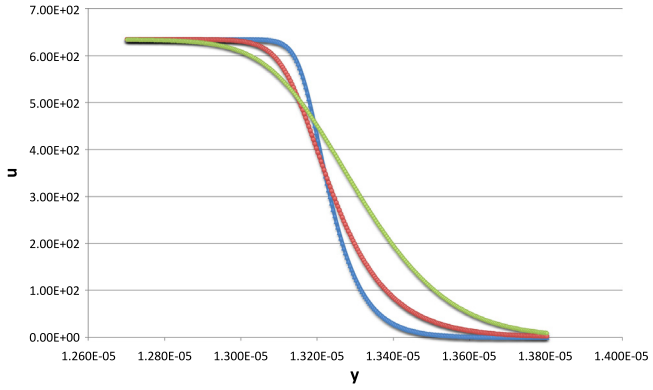

Fig. 3. Velocity field shock profiles are compared for the Mach 3 shock for the three different thermal conductivity cases listed in Section 5.5. Blue curve: case (I), $\mathcal{P} = 0$. Red curve: case (II), $\mathcal{P} = \gamma$. Green curve: case (III), $\bar{\mu}, \kappa \propto T^{0.68}$. (For interpretation of the references to color in this figure legend, the reader is referred to the web version of this article.)

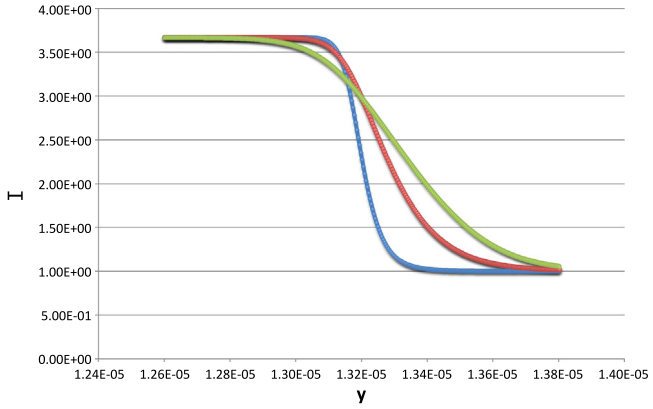

Fig. 4. Shock profiles of normalized internal energy I, where $I \equiv \mathcal{E}/\mathcal{E}_o$, are compared for the Mach 3 shock for the three different thermal conductivity cases listed in Section 5.5. Blue curve: case (I), $\mathcal{P} = 0$. Red curve: case (II), $\mathcal{P} = \gamma$. Green curve: case (III), $\bar{\mu}, \kappa \propto T^{0.68}$. (For interpretation of the references to color in this figure legend, the reader is referred to the web version of this article.)

in the numerical simulations, that is valid for all $0 < \mathcal{P} < \infty$ and all $\mathcal{M} > 1$. In particular, we develop the expansion

$$E(\epsilon) = E_L + a\epsilon + \mathcal{O}(\epsilon^2). \tag{42}$$

Here, E is a dimensionless version of $\mathcal{E}$, $E_L = E(w = \alpha)$ is a known constant, the perturbation coefficient a is determined/discussed in Appendix C, and we have set

$$\epsilon \equiv \frac{u_p - u}{v}, \tag{43}$$

where we observe that $0 < \epsilon \ll 1$ in the region near the piston.

In Figs. 5 and 6, we plot the physically-relevant value of a, the coefficient of the first-order perturbation term, and superpose the results of numerical simulations for four representative values of $\mathcal{P}$.

A general conclusion based on the experimental results of [2,3] is that Navier–Stokes theory more closely represents the measured widths for weak shocks, specifically, those with $\mathcal{M} < 2$, and less closely for stronger shocks. We illustrate the close agreement of theory and simulation vis-à-vis the perturbation coefficient, in both regimes, using $\mathcal{M} = \sqrt{3}$ in Fig. 5 and $\mathcal{M} = 3$ in Fig. 6.

6. Clausius–Duhem and equilibrium thermodynamics

"Once you eliminate the impossible, whatever remains, no matter how improbable, must be the truth". A. Conan Doyle

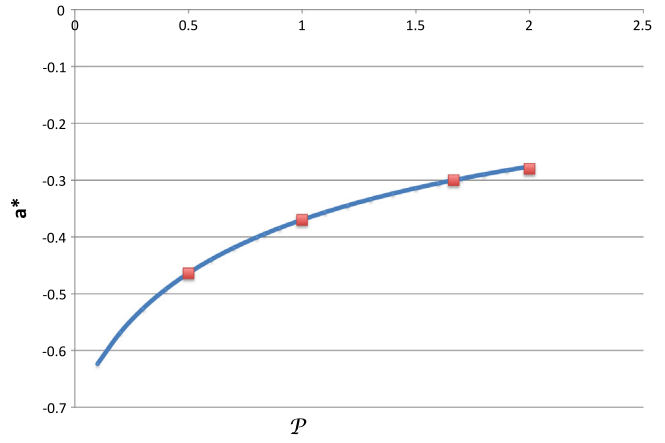

Fig. 5. a^* is plotted as a function of $\mathcal{P}$, for $\gamma = 5/3$ and $\mathcal{M} = \sqrt{3}$. The four red dots are data points plotted from our HIGRAD-generated simulation. (For interpretation of the references to color in this figure legend, the reader is referred to the web version of this article.)

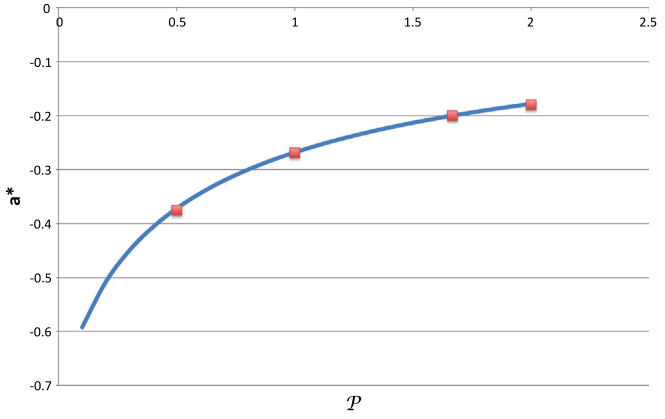

Fig. 6. a^* is plotted as a function of $\mathcal{P}$, for $\gamma = 5/3$ and $\mathcal{M} = 3$. The four red dots are data points plotted from our HIGRAD-generated simulation. (For interpretation of the references to color in this figure legend, the reader is referred to the web version of this article.)

As we have seen, the Becker solution and our self-similar traveling wave solution both show that specific entropy, as given by Eq. (26), has a maximum[3] inside the shock region. This is a sufficiently counter-intuitive result that Morduchow & Libby make special mention of it. Their comment (see [11]) is to the effect that the second law pertains to systems and that entropy downstream of the shock is greater than the entropy upstream, an explanation we find less than convincing.

There is a more "strenuous" test that could be applied to the entropy profile, that test being the Clausius–Duhem inequality (CDI). The CDI [21] is a local form of the second law; it is not about systems, but about individual points of a continuum. The meaning of the CDI is that a physical process should be dissipative at every point. The inequality is most frequently applied to determine the conditions under which a given constitutive relation is thermodynamically allowable.

In differential form, and assuming the absence of heat sources due to external radiation, the CDI reads

$$\rho \frac{DS}{Dt} + \nabla \cdot \left(\frac{\mathbf{q}}{T} \right) \geq 0, \tag{44}$$

where we recall that $\mathbf{q}$ is the heat flux vector and $T(>0)$ is the absolute temperature. In the case of the compressible Navier–Stokes equations, however, the CDI is *identically* satisfied since the LHS of Eq. (44) turns out to be a positive-definite quantity; see, e.g., [17, eq. (2.15)].

It is unfortunate that, in the sense of thermodynamics, a general *nonequilibrium* entropy is not defined [22]. What is given by Eq. (26) is the *equilibrium* entropy, wherein gradients of density, energy, and velocity do not appear. It is interesting that the CDI is more constraining than the global second law by virtue of containing the heat flux which, by Fourier's law, depends on the gradient of the energy. Let us briefly review the derivation of the CDI.

In equilibrium thermodynamics, the local Gibbs equation for a general, single species, fluid reads [17, p. 58]

$$T dS = d\mathcal{E} - \frac{p}{\rho^2} d\rho, \tag{45}$$

which in the case of a perfect gas can be recast as

$$dS = c_v[\mathcal{E}^{-1} d\mathcal{E} - (\gamma - 1)\rho^{-1} d\rho]. \tag{46}$$

The latter form of this relation may be integrated to yield Eq. (26)—but shocks are *not* equilibrium processes. The extension to *classical* irreversible thermodynamics [23] involves two principal assumptions:

- Local thermodynamic equilibrium (LTE)—that small-enough regions of space are in a local equilibrium, so that relations like the equation of state (Eq. (4)) and the Gibbs equation (Eq. (45)) remain valid locally, and the density, velocity, and temperature all become functions of position.
- Local entropy balance—the rate of entropy production in a mass element is described by [17, p. 58]

$$\frac{DS}{Dt} + \rho^{-1}(\nabla \cdot \mathbf{J}^S) = \sigma^S, \tag{47}$$

where $\mathbf{J}^S$ is the entropy flux and σ^S is the per-unit-mass rate of entropy production due to thermoviscous sources within the element. Note that when the entropy flux is taken as $\mathbf{J}^S = \mathbf{q}/T$, and since $\sigma^S \geq 0$ by the second law, Eq. (47) becomes the CDI by replacing "$=\sigma^S$" with "≥ 0".

The motivation for assuming the entropy flux is the heat flux divided by the temperature is based on the definition of entropy in equilibrium thermodynamics. The kinetic theory of gases allows for a more general entropy flux; see, e.g., the discussion in [24]. However, it is the first assumption, that of LTE, with which we will next be concerned.

One of the novel aspects of Becker's [4] analysis is the way he mixes the macroscopic (thermodynamic) and microscopic (gas-kinetic) points of view. Here, we will also adopt this strategy. In the next section we will evaluate the LTE assumption and show that it is valid only for the very weakest shocks. Then, in Section 8, we will take a completely gas-kinetic point of view and calculate the Boltzmann nonequilibrium entropy. We will show that the nonequilibrium entropy is a monotonically increasing function in the shock profile with no internal extrema. Finally, we will propose a purely macroscopic modified entropy that closely estimates the nonequilibrium entropy.

Since from this point forward we will be discussing several different entropies, it is necessary to extend our notation. We will write S^{E} for the equilibrium entropy defined in Eq. (26). We will briefly refer to the generic nonequilibrium entropy of Boltzmann in Eq. (59) as S^{B}. When the Grad approximate solution is used to calculate the Navier–Stokes nonequilibrium entropy in Eq. (62), we will refer to S^{N}. Finally, we will evaluate a modified thermodynamic nonequilibrium entropy S^{M}, which we define below in Eq. (52).

In anticipation of its use in Section 8 and Appendix C, we now rewrite the CDI for the self-similar solution in terms of w. First, we observe that the material time derivative of the equilibrium entropy in Eq. (44) becomes

$$\rho \frac{DS^{\mathrm{E}}}{Dt} = -\rho(v-u)\frac{dS^{\mathrm{E}}}{dy} = -\rho_o v \frac{dw}{dy}\frac{dS^{\mathrm{E}}}{dw}. \tag{48}$$

[3] Actually, this is true for all $\mathcal{P} > 0$ [14], the case $\mathcal{P} = 0$ (i.e., $k = 0$) being the sole exception; see Remark 3 in Appendix B, and also our calculations at the end of Appendix C.

Next, the entropy flux term assumes the form:

$$\frac{\mathbf{q}}{T} = c_v \frac{\mathbf{q}}{\mathcal{E}} = -\frac{\kappa c_v}{\mathcal{E}} \frac{d\mathcal{E}}{dy} = -\kappa c_v \frac{d\ln(\mathcal{E}/\mathcal{E}_o)}{dy} = -\kappa c_v \frac{dw}{dy} \frac{d\ln(\mathcal{E}/\mathcal{E}_o)}{dw}. \tag{49}$$

Thus, it follows that

$$\frac{d}{dy}\left(\frac{\mathbf{q}}{T}\right) = -(\kappa c_v)\frac{dw}{dy}\frac{d}{dw}\left[\left(\frac{dw}{dy}\right)\left(\frac{d\ln(\mathcal{E}/\mathcal{E}_o)}{dw}\right)\right]. \tag{50}$$

And so the CDI for the self-similar shock is

$$\mathrm{CDI} = -\rho_0 v \left(\frac{dw}{dy}\right)\frac{d}{dw}\left(S^{\mathrm{M}}\right) \geq 0. \tag{51}$$

Here, we define

$$S^{\mathrm{M}} \equiv S^{\mathrm{E}} + \frac{c_v \mathcal{P}\ell(\gamma+1)}{2\gamma}\left[\left(\frac{dw}{dy}\right)\left(\frac{d\ln(\mathcal{E}/\mathcal{E}_o)}{dw}\right)\right], \tag{52}$$

where we have made use of the expression for ℓ given in Eq. (18) and the defining relation for $\mathcal{P}$.

Considering Eq. (51) and that our shock is moving to the right, the quantity S^{M} is monotonically increasing through the shock, and thus is a good candidate for a nonequilibrium thermodynamic entropy. To support this hypothesis we will, in Section 8, compare S^{M} directly with S^{N} for a Mach 3 shock.

7. Local thermodynamic equilibrium

"In practice, the criterion for equilibrium is circular. Operationally, a system is in an equilibrium state if its properties are consistently described by thermodynamic theory!" H.B. Callen

The theoretical connection between the Boltzmann equation and Navier–Stokes theory is the Chapman–Enskog (CE) approximation. CE is a perturbation expansion in the Knudsen number, K_n, which is the ratio of molecular mean free path to macroscopic length scale. If a shock is of the order two or three mean free paths wide, then K_n is not small and one should not expect the perturbation approximation to be accurate[4] . In effect, we have come full circle and conclude that *Becker's original concerns are well-founded.* Below, we will make some rough estimates, in the spirit of Becker [4], combining results from Navier–Stokes (continuum) theory and kinetic theory to quantify our conclusions.

A quantitative justification for LTE would be that gradients are small over some macroscopic length scale Δx, specifically,

$$\frac{\Delta x}{\Delta u}\left|\frac{du}{dy}\right| \ll 1, \tag{53}$$

where Δu is the total change in velocity across the shock. For example, in the case of numerical simulation one might interpret Δx as the size of one computational cell. In CE theory, Δx is the (somewhat nebulous) *macroscopic* scale that must be "large" when compared to the molecular mean free path, λ. More generally, Δx is not a scale of the flow, but rather of the observer of the flow; see [25] for elaboration. Eq. (53), we observe, defines an upper bound on Δx.

From a kinetic-physics point of view, it is the collisions that restore an equilibrium distribution to the molecular velocities. So the establishment of local equilibrium also places a lower bound on Δx as a multiple of the molecular mean free path. Numerical studies suggest that the CE-based derivation of the Navier–Stokes system is not justifiable for K_n greater than $\simeq$0.1; see [26]. This, then, leads to the conservative estimate

$$\Delta x_1 \geq 10\lambda. \tag{54}$$

[4] Navier–Stokes theory was formulated empirically many decades before Chapman and Enskog.

A more generous estimate can be made from [2, fig. 2], where the narrowest experimentally measured shock implies

$$\Delta x_2 \geq 3.5\lambda, \tag{55}$$

which we recall is based on $\delta = 5\pi/32$ (see Section 5.4).

Our task now is to determine whether there is a range of *allowable* values of Δx that lies between the lower and upper bounds described above. We will make the following explicit choices: Take $\mathcal{P} = \gamma$, so that we can use the Becker solution in what follows; consider the velocity gradient, in particular, and look near the center of the profile at the point where the magnitude of the velocity gradient is at its maximum; and use the more generous estimate of minimal Knudsen number cited in Eq. (55)[5] .

We begin with Eq. (17), evaluated at $w = w_m = \sqrt{\alpha}$, the point[6] at which $\max|du/dy|_{y\in\mathbb{R}}$ occurs in the solutions of this ODE (and also those of Eq. (37)):

$$\left|\frac{du}{dy}\right| = v\left|\frac{dw}{dy}\right| = \frac{v}{\ell}\left(1-\sqrt{\alpha}\right)^2 = \left(\frac{\rho_o v^2}{\bar{\mu}}\right)\left(\frac{\gamma+1}{2\gamma}\right)\left(1-\sqrt{\alpha}\right)^2,$$

where we recall that α is given in Eq. (19).

Eq. (55) provides a limiting estimate for the macroscale:

$$\Delta x = 3.5\lambda = K_1\sqrt{\gamma}\begin{cases}\left(\dfrac{10\,\bar{\mu}}{\rho_m c_m}\right), & \delta = 0.35,\\ \dfrac{112}{5\pi}\left(\dfrac{\bar{\mu}}{\rho_m c_m}\right), & \delta = 5\pi/32.\end{cases} \tag{56}$$

Here, we have used Eq. (39) to estimate the mean free path, and we have set $K_1 := \frac{3}{4}\sqrt{\pi/8}$ (≈ 0.470). Moreover, ρ_m and c_m represent the density and sound speed, respectively, evaluated at the point $w = w_m$ of the profile; specifically, we have, from Eq. (23),

$$\rho_m = \frac{\rho_o}{\sqrt{\alpha}},$$

while manipulation of Eq. (24) yields

$$c_m = c_o\left[1+\left(\frac{\gamma-1}{\gamma+1}\right)(\mathcal{M}^2-1)\right]^{1/2}.$$

Now taking $\Delta u = v\,\alpha$ and then assembling these results yields

$$\frac{\Delta x}{\Delta u}\left|\frac{du}{dy}\right| \approx \left(\frac{\gamma+1}{2\sqrt{\gamma}}\right)\left(\frac{\mathcal{M}}{\sqrt{\alpha}}\right)\frac{(1-\sqrt{\alpha})^2}{\left[1+\left(\frac{\gamma-1}{\gamma+1}\right)(\mathcal{M}^2-1)\right]^{1/2}} \times K_1\begin{cases}10, & \delta = 0.35,\\ 7.13, & \delta = 5\pi/32.\end{cases} \tag{57}$$

In Fig. 7, the estimate of the (dimensionless) velocity gradient given in Eq. (57) is plotted as a function of the Mach number for two representative values of γ. Given the coarseness of our estimates, one should not look for a single, overall, critical Mach number value. However, it is clear that for monatomic gases, for which $\gamma = 5/3$, LTE will fail by a Mach number of two[7] , which is consistent with detailed comparisons of Navier–Stokes theory and kinetic theory (see, e.g., [27])—More precisely, achieving LTE in monatomic gases requires, based on Eq. (57), that $1 < \mathcal{M} \ll 1.83$ or $1 < \mathcal{M} \ll 2.08$ for $\delta = 0.35, 5\pi/32$, respectively. For more complicated gases such as air, which is a mixture of several components and has a smaller (effective) specific heat ratio of $\gamma \approx 1.4$, LTE will fail at even *smaller* Mach number values; viz.: achieving LTE in diatomic[8] gases, for which $\gamma = 7/5$, demands $1 < \mathcal{M} \ll 1.66$ or $1 < \mathcal{M} \ll 1.81$ for $\delta = 0.35, 5\pi/32$, respectively.

[5] We note that this is consistent with shock-capturing numerical simulations where an artificial viscosity chosen to yield a shock that is between three and four computational cells wide suffices to eliminate unphysical post-shock oscillations; see [16].

[6] Recall that this is also the point where the equilibrium entropy profile (i.e., Eq. (27)) exhibits its maximum; see Section 3.

[7] The mid-20th century consensus was that continuum theory failed for $1.3 \lesssim M_0$; see [1] (wherein M_0 is defined), and the references cited therein, but take note of the lack of consistent schemes for defining $\mathcal{W}$ and assigning a value to δ.

[8] Example of which include H_2, N_2, and O_2; see [17, p. 80].

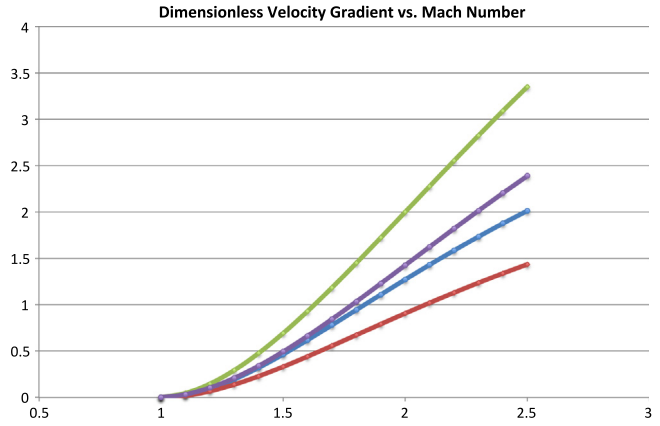

Fig. 7. Dimensionless estimate of the velocity gradient (plotted from Eq. (57)) vs. $\mathcal{M}$ for two representative values of γ and two values of δ. Green curve: $\gamma = 1.4$ and $\delta = 0.35$. Purple curve: $\gamma = 1.4$ and $\delta = 5\pi/32$. Blue curve: $\gamma = 5/3$ and $\delta = 0.35$. Red curve: $\gamma = 5/3$ and $\delta = 5\pi/32$. (For interpretation of the references to color in this figure legend, the reader is referred to the web version of this article.)

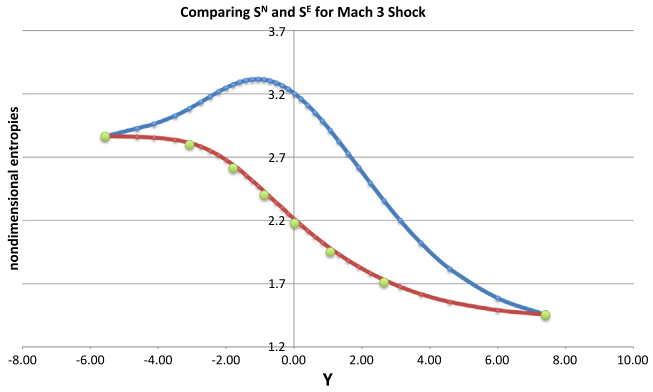

Fig. 8. The nonequilibrium entropy S^N (red curve) is compared with the equilibrium entropy S^E (blue curve), in dimensionless units for the Mach 3 shock. The green dots show a modified S^N in which the viscous term in the velocity PDF is "turned off", illustrating that viscosity plays essentially *no* role in the nonequilibrium entropy. (For interpretation of the references to color in this figure legend, the reader is referred to the web version of this article.)

Remark 2. In solutions of Eq. (17), the center (or midpoint) of the velocity profile is located at $w = w^* = (1+\alpha)/2$ (see Section 5.4) while $\max |du/dy|_{y\in\mathbb{R}}$ occurs at $w = w_m = \sqrt{\alpha}$, where $0 < w_m < w^* < 1$ since $0 < \alpha < 1$.

8. Nonequilibrium entropy

In this section, we will derive a nonequilibrium entropy for the Navier–Stokes equations based on gas kinetic theory. The entropy that appears in Eqs. (26) S^{E} is the thermodynamic *equilibrium* entropy. The extension to nonequilibrium processes is made through the assumption of local thermodynamic equilibrium [23] as described in Section 6. That implies that the macroscopic field quantities, e.g., density, temperature, etc., will depend on the spatial coordinate. However, the gradients of density, energy, etc., do not appear in the equilibrium entropy.

A general nonequilibrium entropy is not defined [22] in classical thermodynamics. However, in the more fundamental descriptions of statistical mechanics and gas kinetic theory, a nonequilibrium entropy can be defined in terms of the velocity probability distribution function (PDF). The H-theorem, introduced by Boltzmann in 1872, describes the tendency for the quantity $\mathcal{H}$ to be monotonically decreasing, where

$$\mathcal{H} \equiv \int f \, \ln(f)\, d^3v, \tag{58}$$

and where $f(x_i, v_i, t)$ is any solution of the Boltzmann equation [28]. In turn, a nonequilibrium entropy, S^{B}, can be defined in terms of $\mathcal{H}$, viz.,

$$S^{\mathrm{B}} \equiv -\int f \, \ln(f)\, d^3v = -\mathcal{H}. \tag{59}$$

Remarkably, when the equilibrium Boltzmann–Maxwell distribution, i.e.,

$$f^{\mathrm{E}}(v) = \rho\Big(\frac{1}{2\pi\mathcal{E}}\Big)^{3/2} \exp\left[-\frac{(v-\bar{v})^2}{2\mathcal{E}}\right], \tag{60}$$

is inserted into Eq. (59), one finds that S^{B} is identical to the thermodynamic entropy, S^{E}, defined in Eq. (26), except for additive constant(s).

Solving the Boltzmann equation for nonequilibrium flows is very difficult, and one is usually constrained to constructing perturbation approximations assuming that the flow is near equilibrium. This is the case for deriving the Navier–Stokes equations. One path from the Boltzmann equation to Navier–Stokes was proposed by Grad [29]. The Grad PDF, f^{G}, is a perturbation of the equilibrium solution of the Boltzmann equation; its derivation is lengthy and intricate (see, e.g., chap. 4 of [28]). Here, we present the Grad PDF with two modifications to ensure the closest comparison with our analysis in Section 2. First, we assume a 1D flow and integrate over the two extraneous dimensions; and second, we introduce the longitudinal viscosity term, σ. This gives us the modified (Grad) PDF:

$$f^{\mathrm{M}}(v) = f^{\mathrm{E}}(v)\left\{1 + \frac{1}{2\rho\mathcal{E}^2}\left[\sigma\,(v^2-\mathcal{E}) + \frac{4}{5}\,qv\left(\frac{v^2}{2\mathcal{E}} - \frac{5}{2}\right)\right]\right\}. \tag{61}$$

Here, we have set $\sigma \equiv -\bar{\mu}\,\partial u/\partial x$, and we recall that $q = -\kappa\,\partial\mathcal{E}/\partial x$ is the heat flux. Note that both the original Grad PDF and our modified version of it are carefully constructed to ensure that the macroscopic variables of density and average velocity are the equilibrium values. This is an essential feature of the assumption of local thermodynamic equilibrium. Now inserting Eq. (61) into (59), we define the nonequilibrium entropy for Navier–Stokes theory:

$$S^{\mathrm{N}} \equiv -\int f^{\mathrm{M}} \ln(f^{\mathrm{M}})\, dv. \tag{62}$$

We have evaluated the integral above numerically using the particular parameters of the Mach 3 shock. The issue at hand is not only to compare the equilibrium and nonequilibrium entropies, but more simply to ascertain whether S^{N} has a maximum inside the shock profile. The answer to the latter is shown graphically in Fig. 8—In contrast to S^{E}, *the nonequilibrium entropy* S^{N} *is monotonically increasing through the shock profile*. Further, as the equilibrium and nonequilibrium entropies must agree in the regions in front of and behind the shock, it is easy to determine the relative scale factors; a direct comparison of the two entropies is also shown in Fig. 8.

There is more to learn from Eq. (61). Let us now remove the contribution of the longitudinal viscosity term from f^{M}, by setting $\sigma = 0$, and recompute the entropy. Representative points added in Fig. 8 show that there was no discernible contribution to S^{N} from the longitudinal viscosity. If, in addition, we now remove the contribution of the heat flux, then what remains is the equilibrium PDF, f^{E}, and the equilibrium entropy, S^{E}; thus, we conclude that the main difference between S^{E} and S^{N} is due to the heat flux q term in Eq. (61).

The importance of the heat flux in the nonequilibrium entropy brings to mind the Clausius–Duhem inequality discussed in Section 6. We conjecture that a nonequilibrium thermodynamic entropy might be accurately estimated for the 1D self-similar solution by including the entropy flux in the entropy. In particular, we focus on the modified thermodynamic entropy defined in Eq. (51). To test this conjecture, we have calculated S^{M} numerically and compared it to S^{M} in Fig. 9. The agreement is not exact, but is compelling. In Appendix C we show that S^{M} is monotonically increasing for all realizable Prandtl and Mach

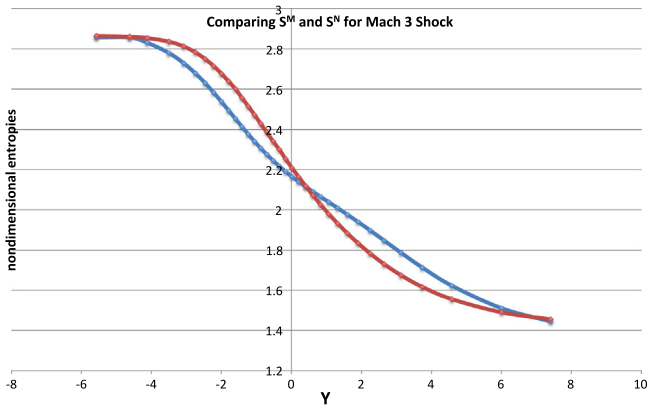

Fig. 9. The nonequilibrium entropy S^{N} (red curve) is compared with the modified equilibrium entropy S^{M} (blue curve), for the Mach 3 shock using dimensionless units. (For interpretation of the references to color in this figure legend, the reader is referred to the web version of this article.)

numbers. A revised CDI has the simple form

$$\frac{dS^{\mathrm{M}}}{dy} \geq 0. \tag{63}$$

Note that this form of the inequality results from self-similarity and is not restricted to only shock waves.

9. Closure

In this paper we have considered the general structure of shock waves calculated by Navier–Stokes theory. In particular, we have studied the distribution of entropy within the shock profile. Our analysis was motivated by two classic papers in shock structure. The first is the 1922 paper by Becker [4] that presented the first steady shock solution of a Navier–Stokes shock that includes both viscosity and heat conduction. Becker used his solution to estimate the shock width and raised the issue that the predicted shock width, measured in units of the molecular mean free path, was too narrow to allow the Chapman–Enskog perturbation theory to converge; i.e., he questioned the use of the Navier–Stokes equations to describe the structure of shocks.

The second is the 1949 paper by Morduchow & Libby [1] that revisited Becker's analysis and calculated the entropy distribution, explicitly showing an entropy maximum within the profile. This is certainly a counter-intuitive result, but the authors concluded that it did not violate the global version of the second law of thermodynamics, namely, that the total entropy of the system must increase.[9]

The principal new results of this paper are five-fold:

1. In Section 2 we derived the self-similar solution in analogy to Becker's steady-shock solution; then, in Section 4, we derived a special case of the former, which appears to be a new result, that corresponds to $\mathcal{M} = \mathcal{M}^*$ and yields a class of exact, explicit, traveling wave solutions valid for all perfect gases. In Section 5, we developed a direct numerical simulation code that solves the compressible Navier–Stokes equations at high resolution. We then compared the numerical solutions with the traveling wave solutions of the self-similar equations. We demonstrated that the numerically and analytically determined solutions are in excellent agreement and, furthermore, that the former is stable from the computational standpoint.
2. Our analysis has also revealed shortcomings in the steady-shock approach vis-à-vis its usefulness in modeling shock experiments. In particular, it is lacking in the sense that, along with that of the velocity (in the form of u_p), the value of at least one[10] state variable must also be specified at $-\infty$; in the case of [1], it is T, which creates a formulation inconsistency since the face of the piston is tacitly assumed to be insulated. This is in contrast to the present traveling wave-based analysis of the piston problem, wherein only the value of the velocity must be specified at $-\infty$, while those of the state variables (and the velocity) must be given at $+\infty$. The latter approach is thus more realistic from the modeling standpoint; indeed, an experimenter, who clearly has control over the speed of the piston and the state of the gas ahead of the shock, would perform the shock experiment in order to *determine* the values of ρ, T, and p at the piston. This problem with the steady-shock approach is manifested in [1] in at least two other ways: (i) the state of the gas at $+\infty$ cannot be independently specified, i.e., it depends on the conditions at $-\infty$; and (ii), the entropy profile in [1, fig. 3] is the reverse-image of that given above in Fig. 2, a consequence of the fact that the temperature at the face of the piston in [1] is *less* than it is at $+\infty$.
3. In Section 7, we quantified the meaning of LTE (in the spirit of Becker) and showed that it is a valid assumption for only the very weakest of shocks, i.e., those well-described by weakly-nonlinear theory (see Appendix A.2). This is an important result in the following sense: There are no length scales in classical thermodynamics; however, the derivation of the (compressible) Navier–Stokes equations from kinetic theory requires two assumptions that place first a lower and then an upper limit on system size. On the one hand, there must be sufficient collisions to allow equilibration (lower bound), while on the other hand macroscopic properties must not change significantly over the collision process (upper bound). In the case of shocks in monatomic gases, our most "charitable" estimate indicates that these bounds are *incompatible* for shock strengths of $2 \lesssim \mathcal{M}$.
4. In Section 8 we calculated directly the gas-kinetic entropy, S^{N}, for the Navier–Stokes solutions and showed that it is significantly different from the equilibrium entropy, S^{E}. Indeed, S^{N} is monotonically increasing through the shock profile in accordance with our intuition. We do not believe the structure of the equilibrium entropy has any significance in Navier–Stokes theory.
5. We have hypothesized a nonequilibrium thermodynamic entropy, i.e., one that depends on macroscopic variables, that is monotonically increasing through the shock, and which closely estimates the nonequilibrium Boltzmann entropy that is based on the statistical mechanical probability distribution function. Our hypothesis is currently restricted to self-similar flows, but is not necessarily restricted to shocks due to its relation to the Clausius–Duhem inequality.

Becker's paper [4] called into question the applicability of Navier–Stokes theory to shocks only a few years after the Chapman–Enskog expansion was introduced. The validity of his criticisms is now well established by experiment. However, the search for a more accurate replacement remains an active research topic.

Acknowledgments

We gratefully acknowledge discussions with Brian Albright, Roy Baty, Darryl Holm, Marshall Slemrod and Francisco Uribe. The authors thank Josette P. Fabre for carefully proofreading an earlier version

[9] The term entropy is used in many different contexts, thermodynamics, statistical mechanics, PDE theory, numerical methods, chaos theory, topology, etc. [30]. The relationship among these many concepts is in general not known.

[10] While the values of T and either p or ρ at $-\infty$ are needed to *explicitly* determine C_1 and C_3, which are constants of integration (see [1, eqs. (8a), (8b)]), only T_0 and u_0, where Morduchow & Libby attach a zero subscript to a flow quantity to denote the value of that quantity at $-\infty$, appear in [1, eq. (12b)], their equation of motion.

of this manuscript. LGM and JMR were supported by the Los Alamos National Laboratory operated by Los Alamos National Security, LLC under contract number DE-AC52-06NA25396. PMJ was supported by ONR/NRL funding.

Appendix A. Approximate and asymptotic results

The derivations presented in this appendix are most readily carried out by recasting Eq. (17) in the form

$$(\chi-\psi)\frac{d\psi}{dY}=-(1-\psi^2). \tag{A.1}$$

Here, we have set $w\equiv 1-\frac{1}{2}(1-\alpha)(1+\psi)$; the parameter χ is defined as

$$\chi\equiv\frac{1+\alpha}{1-\alpha}=\frac{1+\gamma\mathcal{M}^2}{\mathcal{M}^2-1}, \tag{A.2}$$

where we observe that $\chi>1$; and we introduce the dimensionless similarity variable $Y\equiv y/\ell$.

Before beginning our analysis it should be noted that, while originally derived for the Becker case (i.e., $\mathcal{P}=\gamma$), all results presented in this appendix are easily made to apply to the case $\mathcal{P}=0$ (see Remark 1) by replacing ℓ with ℓ/γ in the defining relation for Y.

A.1. Results for all $\mathcal{M}>1$

With our equation of motion in the form of Eq. (A.1), it is a straightforward matter to apply the results given in [31, §5.2] and derive the following (explicit) approximation to the Becker solution:

$$u(Y)\approx u_p\begin{cases}1-\dfrac{\chi-1}{\chi+1}W_0\left[\left(\dfrac{\chi+1}{\chi-1}\right)\exp\left(\dfrac{2(Y+\ln 2)}{\chi-1}\right)\right], & Y\ll Y_1,\\ \frac{1}{2}\left(1+\chi-\sqrt{\chi^2+2Y}\right), & |Y|\ll\chi,\\ \dfrac{\chi+1}{\chi-1}W_0\left[\left(\dfrac{\chi-1}{\chi+1}\right)\exp\left(\dfrac{-2(Y+\ln 2)}{\chi+1}\right)\right], & Y\gg Y_2,\end{cases} \tag{A.3}$$

where $W_0(\cdot)$ denotes the principal branch of the Lambert W-function, and we have set $Y_{1,2}\equiv-\ln(2)\mp(\chi\mp 1)/2$.

From Eq. (A.3) and the fact that $W_0(x)\sim x-x^2$, as $x\to 0$, the following asymptotic expressions are easily obtained:

$$u(Y)\sim u_p\times\begin{cases}1-\exp\left(\dfrac{-2|Y|}{\chi-1}\right)\left[1-\dfrac{\chi+1}{\chi-1}\exp\left(\dfrac{-2|Y|}{\chi-1}\right)\right], & Y\to-\infty,\\ \frac{1}{2}\left(1-Y/\chi+\frac{1}{2}Y^2/\chi^3\right), & |Y|\to 0,\\ \exp\left(\dfrac{-2Y}{\chi+1}\right)\left[1-\dfrac{\chi-1}{\chi+1}\exp\left(\dfrac{-2Y}{\chi+1}\right)\right], & Y\to\infty.\end{cases} \tag{A.4}$$

From these expressions, we are able to quantify the kink's asymmetric shape in the large-$|Y|$ regimes; qualitatively, however, its clear that the rate at which $u(Y)$ tends to u_p (i.e., its left-asymptotic limit) is *faster* than that which it tends to zero (i.e., its right-asymptotic limit).

A.2. Results for weak shocks

What are referred to above as "weak shocks", i.e., those for which $1<\mathcal{M}\ll 2$, result when $u_p\ll c_o$. This is easily established by recasting the RHS of Eq. (21) in terms of u_p/c_o and expanding, viz.:

$$\mathcal{M}\approx 1+\tfrac{1}{4}(\gamma+1)(u_p/c_o)+\tfrac{1}{32}(\gamma+1)^2(u_p/c_o)^2\quad(u_p\ll c_o), \tag{A.5}$$

where we observe that $\mathcal{M}>u_p/c_o$.

In the broader context, the assumption $M_p\ll 1$ is the basis of weakly-nonlinear compressible flow theory, the aim of which is to derive simplified (i.e., approximate) versions of the compressible Navier–Stokes system that still capture the salient physics of the flow in question; see, e.g., [9] and the references cited therein. In the present study, M_p may be called the piston Mach number, because $M_p=u_p/c_o$; for compressible flows in general, however, it is sometimes referred to as the "peak particle velocity Mach number" (of the flow).

In the case of weak shocks, where we observe that

$$M_p\ll 1\quad\Rightarrow\quad 1<\mathcal{M}\ll 2\quad\Rightarrow\quad\chi\gg 1, \tag{A.6}$$

$u(Y)$ exhibits Taylor shock-like behavior, specifically,

$$u(Y)\approx\tfrac{1}{2}u_p[1-\tanh(Y/\chi)]\quad(\chi\gg 1), \tag{A.7}$$

which unlike the (exact) profiles corresponding to the piecewise-valid approximations above is symmetric[11] . It is noteworthy that by re-expressing it in terms of y/ℓ, and then approximating the resulting quotient $\chi/\mathcal{M}$ to $\mathcal{O}(1/M_p)$, under the weakly-nonlinear scheme, Eq. (A.7) becomes the velocity traveling wave solution of the Becker case of the (weakly-nonlinear) PDE known as the *Blackstock–Lesser–Seebass–Crighton* (BLSC) equation [31, §4].

Appendix B. Expressions valid for arbitrary values of $\mathcal{P}$

The results presented in this appendix are intended to lay the groundwork for further study of shock phenomena, in particular, the general case $\mathcal{P}\neq 0,\gamma,\infty$, using the similarity variable (i.e., traveling wave) approach. To this end, we observe that for arbitrary values of $\mathcal{P}\geq 0$, the elimination of ρ and $\mathcal{E}$ between Eqs. (9), (10), and (11) yields the general equation of motion

$$(1-w)(w-\alpha)=\begin{cases}\left[1+\mathcal{P}\left(\dfrac{\mathcal{M}^2-\gamma^{-1}}{\mathcal{M}^2}\right)-(1+2\mathcal{P})(1-w)\right]\\ \quad\times\left(\dfrac{\ell}{\gamma}\right)\dfrac{dw}{dy}+\dfrac{l\ell}{\gamma}\left[\left(\dfrac{dw}{dy}\right)^2+w\left(\dfrac{d^2w}{dy^2}\right)\right], & \mathcal{P}\neq\gamma,\\ -\dfrac{4l}{\gamma+1}\left(\dfrac{\mathcal{M}^2+\gamma^{-1}}{2\mathcal{M}^2}-w\right)\dfrac{dw}{dy}, & \mathcal{P}=\infty,\end{cases} \tag{B.1}$$

where we recall that Eq. (17) corresponds to the case $\mathcal{P}=\gamma$. Here, we have set $l=\kappa/(\rho_o v)$, and we note that the cases $\mathcal{P}=\infty$ and $\mathcal{P}=0$ imply $\bar{\mu}=0$ and $k=0$, respectively, where we also recall that $\kappa=k/c_v$.

It is noteworthy that Eq. (B.1) is the traveling wave (i.e., self-similar) version of the equations of motion given by Rayleigh [6, eq. (97)] and Taylor [7, eq. (6)] in 1910, both of whom applied the steady-state shock approach to the piston problem. It is also noteworthy to compare the $\mathcal{P}\neq 0,\gamma,\infty$ case of Eq. (B.1) with its third-order counterpart given by Christov et al. [31, eq. (22)], an ODE which is also based on the traveling wave assumption; evidently, employing the entropy balance equation [17, eq. (2.16)], in place of the total energy equation (i.e., Eq. (3)), yields an equation of motion for the traveling wave version of the piston problem that is *one* order greater.

And recalling that Eqs. (10) and (26) hold for all perfect gases, regardless of Prandtl number, we observe the following: With the aid of Eq. (23), the former and latter can be written in terms of w as

$$\mathcal{E}=\mathcal{E}_o\left[(1+\gamma\mathcal{M}^2)-\gamma\mathcal{M}^2w-\tfrac{1}{2}\ell(\gamma+1)\mathcal{M}^2\frac{dw}{dy}\right]w, \tag{B.2}$$

$$\frac{S-S_o}{c_v}=\ln\left[-\tfrac{1}{2}(\gamma+1)\ell\mathcal{M}^2\left(\frac{dw}{dy}\right)+(1+\gamma\mathcal{M}^2(1-w))\right]+\gamma\ln(w). \tag{B.3}$$

Remark 3. On setting $k=0$, Eq. (B.3) reduces to

$$\frac{S-S_o}{c_v}=\ln\left[-\tfrac{1}{2}\gamma(\gamma+1)\mathcal{M}^2(1-w)(w-\alpha)+(1+\gamma\mathcal{M}^2(1-w))w\right]+(\gamma-1)\ln(w)\quad(\mathcal{P}=0), \tag{B.4}$$

[11] In the sense that both $u=u_p/2$, the midpoint of the profile, and $\max|du/dY|_{Y\in\mathbb{R}}$ occur at the *same* Y-value, i.e., $Y=0$.

which we have simplified with the aid of Eq. (37). It can be shown that for this special case, and only this special case, the specific entropy profile assumes the form of a strictly positive, strictly decreasing, kink, and as such does *not*[12] exhibit a stationary point.

Appendix C. Perturbation solution

The purpose of this appendix is to derive a *general* representation of the specific internal energy $\mathcal{E}$ as a function of the velocity in the post shock region of the flow, where $u = v(1-w) \approx v(1-\alpha)$. Hence, assuming only that $0 < \mathcal{P} < \infty$, we return to the self-similar Eqs. (5)–(7), and the equation of state (8), which are repeated below:

$$\rho(v-u) = \rho_o v, \tag{C.1}$$

$$u\rho(v-u) - (\gamma-1)\rho\mathcal{E} + \bar{\mu}\frac{du}{dy} = -p_o, \tag{C.2}$$

$$\rho\mathcal{E}(v-u) + \frac{1}{2}\rho u^2(v-u) - (\gamma-1)\rho\mathcal{E}u + \bar{\mu}u\frac{du}{dy} + \kappa\frac{d\mathcal{E}}{dy} = v\mathcal{E}_o\rho_o, \tag{C.3}$$

$$p = (\gamma-1)\rho\mathcal{E}. \tag{C.4}$$

As in Section 2, we use the mass conservation equation (Eq. (C.1)) to eliminate ρ from the momentum equation (Eq. (C.2)), the result of which we write as

$$w + (\gamma-1)\frac{E}{w} + \frac{dw}{dz} = (\gamma-1)E_o + 1 \equiv A. \tag{C.5}$$

Here, we introduce $E \equiv \mathcal{E}/v^2$, the nondimensional specific internal energy, and $z \equiv (\rho_o v/\bar{\mu})\, y$. Then

$$\frac{dw}{dz} = \frac{1}{w}\frac{d}{dz}\left[\frac{w^2}{2}\right] = Aw - w^2 - (\gamma-1)E. \tag{C.6}$$

where we observe that

$$E_o = \frac{c_o^2}{\gamma v^2(\gamma-1)} = \frac{1}{\gamma(\gamma-1)\mathcal{M}^2}, \tag{C.7}$$

and where we recall that c_o is the sound speed at $w = 1$ and $\mathcal{M}$ is the Mach number.

Next, we turn to the energy equation:

$$\gamma E + \frac{1}{2}w^2 + \frac{d}{dz}\left[\mathcal{P}E + \frac{1}{2}w^2\right] = \gamma E_o + \frac{1}{2} \equiv B. \tag{C.8}$$

In the Becker solution, $\mathcal{P} = \gamma$; here, we treat it as a positive constant. We now use the chain rule to write

$$\frac{dE}{dz} = \frac{dE}{dw}\frac{dw}{dz}.$$

Then

$$\begin{aligned}\frac{d}{dz}\left[\mathcal{P}E + \frac{1}{2}w^2\right] &= \left[\frac{\mathcal{P}}{w}\frac{dE}{dw} + 1\right]\frac{dw}{dz} \\ &= \left[\frac{\mathcal{P}}{w}\frac{dE}{dw} + 1\right]\left[Aw - w^2 - (\gamma-1)E\right].\end{aligned} \tag{C.9}$$

Thus, Eq. (C.8) may be written as the following ODE in E and w:

$$\left[\gamma Ew + \frac{1}{2}w^3 - Bw\right] + \left[\mathcal{P}\frac{dE}{dw} + w\right]\cdot\left[Aw - w^2 - (\gamma-1)E\right] = 0. \tag{C.10}$$

Eqs. (C.5) and (C.10) are still completely general, both in the sense that they are valid for the entire domain of the shock and also that they contain $\mathcal{P}$, $\mathcal{M}$, and γ as unspecified parameters. Rather than seek a complete solution, we now construct an approximate solution near the asymptotic value $w = \alpha$. (In the simulations, this is the region near the piston; in terms of our Fig. 2, this is the region where the entropy is decreasing as we move to the left.)

[12] Since they assumed k (as well as $\bar{\mu}$) to be strictly positive, this result does not contradict the proof given by Serrin & Whang [14].

For our purposes we need only evaluate the perturbation expansion to first order; i.e., approximate Eq. (42) by

$$E \approx E_L + a\epsilon, \tag{C.11}$$

where determining the coefficient a will the primary goal of this appendix, and we note that $E_L = \mathcal{E}_L/v^2$. To this end we return to Eq. (43) and, using the defining relation for w, write

$$w = (1-u_p/v) + \epsilon = \alpha + \epsilon \quad \Rightarrow \quad \frac{d}{dw} = \frac{d}{d\epsilon}.$$

Here, we recall that $0 < \epsilon \ll 1$ in the region near the piston and that $\alpha = 1 - u_p/v$.

In the momentum equation (Eq. (C.5)) we set $w = \alpha$,

$$(\gamma-1)E_L = A\alpha - \alpha^2. \tag{C.12}$$

Equivalently, from the energy equation (C.8),

$$\gamma E_L = B - \frac{1}{2}\alpha^2. \tag{C.13}$$

These relationships show that the constants A, B, and α are not independent. Also, to $\mathcal{O}(\epsilon)$,

$$w = \alpha + \epsilon; \qquad w^2 = \alpha^2 + 2\alpha\epsilon;$$

$$w^3 = \alpha^3 + 3\alpha^2\epsilon; \qquad \frac{dE}{dw} = a.$$

Note that the monotonicity of E as a function of w, proven in Section 3, indicates that $a \le 0$.

Returning to Eq. (C.5), we substitute for the energy term, and this yields

$$\frac{dw}{dz} \approx Aw - w^2 - (\gamma-1)(E_L + a\epsilon) = [A - 2\alpha - (\gamma-1)a]\,\epsilon. \tag{C.14}$$

Then,

$$\frac{d}{dw}\left(\frac{dw}{dz}\right) = [A - 2\alpha - (\gamma-1)a]; \tag{C.15}$$

thus, $\frac{dw}{dz} \sim \mathcal{O}(\epsilon)$ and $\frac{d}{dw}\left(\frac{dw}{dz}\right) \sim \mathcal{O}(1)$.

Now we can rewrite the energy equation (C.10) to first order. For example, the sum in the first set of brackets on the LHS of Eq. (C.10) becomes

$$\begin{aligned}\gamma Ew + \frac{1}{2}w^3 - Bw = &\left[\alpha\gamma E_L + \frac{1}{2}\alpha^3 - B\alpha\right] \\ &+ \left[\gamma(a\alpha + E_L) + \frac{3}{2}\alpha^2 - B\right]\epsilon.\end{aligned} \tag{C.16}$$

Here, the first term on the RHS vanishes exactly, a consequence of the asymptotic condition. Further simplification then results from using Eq. (C.13):

$$\gamma Ew + \frac{1}{2}w^3 - Bw = \left[\gamma a\alpha + \alpha^2\right]\epsilon, \tag{C.17}$$

while the second bracket set in Eq. (C.10) becomes

$$\left[\mathcal{P}\frac{dE}{dw} + w\right] = [\mathcal{P}a + \alpha] + \epsilon. \tag{C.18}$$

Finally, consider the expression inside the last set of brackets in Eq. (C.10); it becomes

$$\begin{aligned}\left[Aw - w^2 - (\gamma-1)E\right] = &\left[A\alpha - \alpha^2 - (\gamma-1)E_L\right] \\ &+ [A - 2\alpha - (\gamma-1)a]\,\epsilon.\end{aligned} \tag{C.19}$$

Here again, the expression inside the first set of brackets vanishes identically. Now in Eq. (C.10), there are no terms of $\mathcal{O}(1)$. Equating terms of $\mathcal{O}(\epsilon)$ then leads to our principal result, a quadratic equation

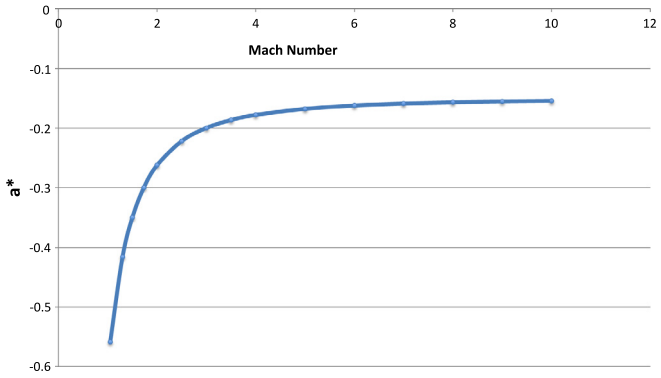

Fig. 10. a^* is plotted as a function of $\mathcal{M}$, for $\gamma = 5/3$ and $\mathcal{P} = 5/3$.

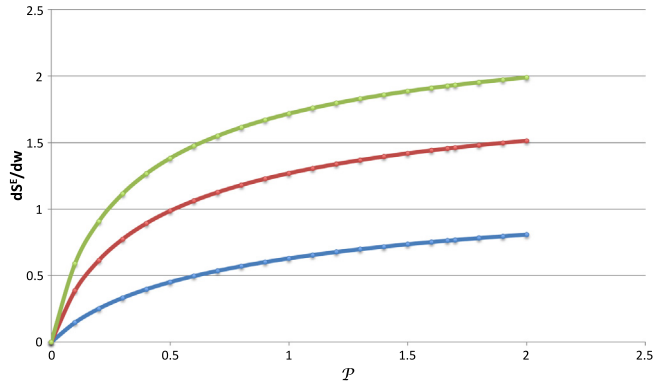

Fig. 11. dS^{E}/dw, the slope of the equilibrium entropy profile, is plotted as a function of $\mathcal{P}$ near the piston's face. Blue curve: $\mathcal{M} = \sqrt{3}$. Red curve: $\mathcal{M} = 3$, Green curve: $\mathcal{M} = 6$. Note that w increases to the right and the shock is moving to the right; therefore, entropy is increasing toward the right. Since the entropy must eventually decrease to the value of the un-shocked gas, this indicates the presence of (at least) one maximum within the profile. (For interpretation of the references to color in this figure legend, the reader is referred to the web version of this article.)

for a:

$$-(\gamma-1)\mathcal{P}a^2 + \Big[\alpha + \mathcal{P}(A-2\alpha)\Big]a + \Big(A\alpha - \alpha^2\Big) = 0. \tag{C.20}$$

With regard to Eq. (C.20), we observe the following:

- The coefficient a depends on three parameters: γ, $\mathcal{P}$, and the shock strength as measured either by $\mathcal{M}$ or by α. To show that the constants A and B depend only on two parameters, namely, γ and α, recall[13]

  $$\alpha = \frac{\gamma-1}{\gamma+1} + \frac{2}{\gamma+1}\frac{1}{\mathcal{M}^2};$$

  thus,

  $$\frac{1}{\mathcal{M}^2} = \frac{(\gamma+1)\alpha}{2} - \frac{\gamma-1}{2}.$$

  Hence,

  $$A = 1 + \frac{1}{\gamma\mathcal{M}^2} = \frac{\gamma+1}{2\gamma}(\alpha+1), \tag{C.21}$$

  from which we see that $A > 1$, and, similarly,

  $$B = \frac{1}{2} + \frac{1}{(\gamma-1)\mathcal{M}^2} = \frac{(\gamma+1)\alpha}{2(\gamma-1)}. \tag{C.22}$$

[13] This relation was derived in Section 2 for the special case of $\mathcal{P} = \gamma$. However, it can easily be shown to depend only on the asymptotic conditions and is independent of $\mathcal{P}$.

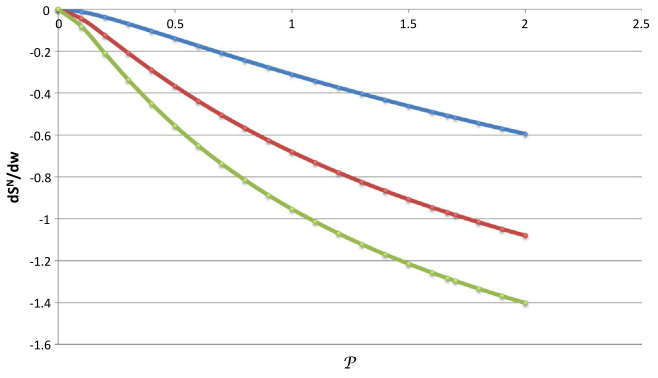

Fig. 12. dS^{N}/dw, the slope of the nonequilibrium entropy profile, is plotted as a function of $\mathcal{P}$ near the piston's face. Blue curve: $\mathcal{M} = \sqrt{3}$. Red curve: $\mathcal{M} = 3$, Green curve: $\mathcal{M} = 6$. Note that w increases to the right and the shock is moving to the right; therefore, the nonequilibrium entropy is decreasing to the right. This is consistent with the monotonicity of the Boltzmann entropy (see Section 8), though it does not necessarily rule out more complicated dependencies. (For interpretation of the references to color in this figure legend, the reader is referred to the web version of this article.)

- The solutions (i.e., roots) of Eq. (C.20) are real-valued. This is readily shown by observing that $A - \alpha > 0$, which follows from Eq. (C.21) and the fact that $0 < \alpha < 1$, while the coefficient of the a^2 term is strictly negative. Hence, provided the coefficient of a is real-valued, which is clearly the case for all realizable values of the physical parameters, it follows by Descartes' rule of signs that Eq. (C.20) admits exactly one negative and one positive root. Moreover, since the discriminant of Eq. (C.20) is strictly positive, i.e., $\Delta > 0$, where

  $$\Delta \equiv \Big[\alpha + \mathcal{P}(A-2\alpha)\Big]^2 + 4\mathcal{P}\alpha(\gamma-1)(A-\alpha), \tag{C.23}$$

  it also follows that these two roots are of single multiplicity (i.e., they maintain their distinct signs); therefore, the two can never coalesce into a single root of multiplicity two at zero, nor any other value of a.
- For the particular case of the Becker solution, the physical solution is the negative root. Thus, the negative root, which we shall henceforth denote as a^*, must be the physical solution for all realizable values of γ, $\mathcal{P}$, and α; this is consistent with the results of Section 3, where it was proven that $\mathcal{E}$ is monotonically decreasing for the entire range of y values.
- Letting $\Pi(a)$ denote the LHS of Eq. (C.20), it is readily established that $\Pi(0) > 0$ while $\Pi(-1) < 0$; therefore, the value of a^* is restricted to the interval $(-1, 0)$ for all realizable values of the physical parameters.
- It is easy to verify that Eq. (C.20) is consistent with the self-similar solution corresponding to $\mathcal{P} = \gamma$. Recall that this special case leads to the invariant (see Eq. (16))

  $$\gamma E + \frac{1}{2}w^2 = \gamma E_o + \frac{1}{2}.$$

  So, near the left asymptotic limit, where $w \approx \alpha + \epsilon$,

  $$\gamma E \approx \gamma E_o + \frac{1}{2}(1-\alpha^2) - \alpha\epsilon,$$

  and thus $a^* = -\alpha/\gamma$. This means that $0 < \frac{3}{5}\alpha \le |a^*| < \alpha < 1$ for perfect gases under Becker's special case, with $\min|a^*|$ occurring in the case of monatomic (i.e., $\gamma = 5/3$) gases. Direct substitution shows that this value of $\mathcal{P}$ and $a = a^*$ satisfy Eq. (C.20).

Plots of the solutions of Eq. (C.20) in Figs. 5 and 6 verify that a^* is negative for $\mathcal{P}$ ranging from 0 to at least 2, for both a weak shock, $\mathcal{M} = \sqrt{3}$, and a stronger shock, $\mathcal{M} = 3$. Particular points on these graphs show the agreement of the theory with representative values taken from

our numerical simulations. Finally, in Fig. 10, a^* is plotted as a function of the Mach number for $\gamma = 5/3$ and $\mathcal{P} = 5/3$.

We can use these results to evaluate $\frac{dS^{\mathrm{E}}}{dy}$ and $\frac{dS^{\mathrm{M}}}{dy}$ in the region near the piston for $\mathcal{P} \neq \gamma$. (Recall that in all our calculations, the shock is moving toward the right.) In Fig. 11 we plot the slope of the equilibrium entropy vs. $\mathcal{P}$ for three values of shock strength. In each case, the slope is positive, meaning that entropy is increasing to the right. Since the equilibrium entropy is smallest in the undisturbed region, far to the right of the shock, we conclude that the equilibrium entropy profile always exhibits at least one maximum, provided $\mathcal{P} > 0$.

In Fig. 12, we plot the slope of the modified entropy S^{M}, which we have suggested as a thermodynamic estimate of the nonequilibrium entropy; see Eq. (51). In this graph, the slope is negative for all finite values of $\mathcal{P}$, meaning that entropy is increasing toward the piston face. This does not exclude the possibility of more complicated distributions, but rules out the simple profiles of Morduchow & Libby.

References

[1] M. Morduchow, P.A. Libby, On a complete solution of the one-dimensional flow equations of a viscous, heat-conducting, compressible gas, J. Aeronaut. Sci. 16 (1949) 674–684 and 704.

[2] H. Alsmeyer, Density profiles in argon and nitrogen shock waves measured by the absorption of an electron beam, J. Fluid Mech. 74 (1976) 497–513.

[3] B. Schmidt, Electron beam density measurements in shock waves in argon, J. Fluid Mech. 39 (1969) 361–373.

[4] R. Becker, Stoßbwelle und detonation (in German), Z. Physik 8 (1922) 321–362 [English transl.: Impact waves and detonation, Part I, N.A.C.A. Technical Memo. No. 505 (N.A.C.A. Washington, DC, 1929); Part II, N.A.C.A. Technical Memo. No. 506 (N.A.C.A. Washington, DC, 1929)].

[5] F.J. Uribe, The shock wave problem revisited: the Navier–Stokes equations and Brenner's two velocity hydrodynamics, in: A.N. Gorban, D. Roose (Eds.), Coping with Complexity: Model Reduction and Data Analysis, Springer, 2011, pp. 207–233.

[6] Lord Rayleigh, Aerial plane waves of finite amplitude, Proc. R. Soc. Lond. Ser. A 84 (1910) 247–284.

[7] G.I. Taylor, The conditions necessary for discontinuous motion in gases, Proc. R. Soc. Lond. Ser. A 84 (1910) 371–377.

[8] H.W. Liepmann, R. Narasimha, M.T. Chahine, Structure of a plane shock layer, Phys. Fluids 5 (1962) 1313–1324.

[9] R. Brunnhuber, P.M. Jordan, On the reduction of Blackstock's model of thermoviscous compressible flow via Becker's assumption, Internat. J. Non-Linear Mech. 78 (2016) 131–132.

[10] W.D. Hayes, Gasdynamic Discontinuities, Princeton University Press, 1960, §D,5.

[11] M. Morduchow, P.A. Libby, On the distribution of entropy through a shock wave, J. de Mécanique 4 (1965) 191–211.

[12] M. Roy, Sur la structure de l'onde de choc, limite d'une quasi-onde de choc dans un fluide compressible et visqueux (in French), C. R. Acad. Sci. 218 (1944) 813–816.

[13] G.S. Golitsyn, K.P. Staniukovich, Some remarks on the structure of shock waves, Sov. Phys.—JETP 8 (1959) 575–576.

[14] J. Serrin, Y.C. Whang, On the entropy change through a shock layer, J. Aeronaut. Sci. 28 (1961) 990–991.

[15] J. von Neumann, R.D. Richtmyer, A method for the numerical calculation of hydrodynamic shocks, J. Appl. Phys. 21 (1950) 232–237.

[16] M.L. Wilkins, Use of artificial viscosity in multidimensional fluid dynamic calculations, J. Comput. Phys. 36 (1980) 281–303.

[17] P.A. Thompson, Compressible-Fluid Dynamics, McGraw–Hill, 1972. [On p. 58, second ¶, the reference to "(2.10)" should read "(2.13)" and on p. 59, "$\mathbf{q} = -\nabla T$" should read "$\mathbf{q} = -\kappa\nabla T$".]

[18] L.H. Thomas, Note on Becker's theory of the shock front, J. Chem. Phys. 12 (1944) 449–453.

[19] K.T. Alligood, T.D. Sauer, J.A. Yorke, Chaos: An Introduction to Dynamical Systems, Springer, 2000, pp. 331–333.

[20] L.G. Margolin, J.M. Reisner, Fully compressible solutions for early stage Richtmyer–Meshkov instability, Comput. Fluids 151 (2016) 46–57.

[21] B.D. Coleman, W. Noll, The thermodynamics of elastic materials with heat conduction and viscosity, Arch. Ration. Mech. Anal. 13 (1963) 167–178.

[22] R.M. Velasco, L.S. García-Colín, F.J. Uribe, Entropy production: its role in nonequilibrium thermodyamics, Entropy 13 (2011) 82–116.

[23] S.R. de Groot, P. Mazur, Non-Equilibrium Thermodynamics, North–Holland, 1962.

[24] I. Müller, On the entropy inequality, Arch. Ration. Mech. Anal. 2 (1967) 118–141.

[25] L.G. Margolin, Finite scale theory: the role of the observer in classical fluid flow, Mech. Res. Comm. 57 (2014) 10–17.

[26] K. Xu, E. Josyula, Continuum formulation for non-equilibrium shock structure calculation, Commun. Comput. Phys. 1 (2006) 425–450.

[27] J.M. Reese, L.C. Woods, F.J.P. Thivet, S.M. Candel, The inner shock structure determined from a modified frame-independent second-order kinetic theory, in: R. Brun, L.Z. Dumitrescu (Eds.), Shock Waves @ Marseille IV: Shock Structure and Kinematics, Blast Waves and Detonations, Springer, 1995, pp. 51–56.

[28] G.M. Kremer, An Introduction to the Boltzmann Equation and Transport Processes in Gases, Springer, 2010.

[29] H. Grad, Principles of the kinetic theory of gases, in: S. Flügge (Ed.), Handbuch der Physik, Vol. XII, Springer–Verlag, 1958, pp. 205–294.

[30] A. Wehrl, The many facets of entropy, Rep. Math. Phys. 30 (1991) 119–129.

[31] I.C. Christov, P.M. Jordan, S.A. Chin-Bing, A. Warn-Varnas, Acoustic traveling waves in thermoviscous perfect gases: kinks, acceleration waves, and shocks under the Taylor–Lighthill balance, Math. Comput. Simulation 127 (2016) 2–18.